The Astronomical Journal, 151:142 (19pp), 2016 June doi:10.3847/0004-6256/151/6/142

UPPER LIMITS FROM FIVE YEARS OF BLAZAR OBSERVATIONS WITH THE VERITAS CHERENKOV TELESCOPES

S. Archambault[1], A. Archer[2], W. Benbow[3], R. Bird[4], J. Biteau[5], M. Buchovecky[6], J. H. Buckley[2], V. Bugaev[2], K. Byrum[7], M. Cerruti[3,31], X. Chen[8,9], L. Ciupik[10], M. P. Connolly[11], W. Cui[12], J. D. Eisch[13], M. Errando[14], A. Falcone[15], Q. Feng[12], J. P. Finley[12], H. Fleischhack[9], P. Fortin[3], L. Fortson[16], A. Furniss[17], G. H. Gillanders[11], S. Griffin[1], J. Grube[10], G. Gyuk[10], M. Hütten[9], N. Håkansson[8], D. Hanna[1], J. Holder[18], T. B. Humensky[19], C. A. Johnson[5], P. Kaaret[20], P. Kar[21], N. Kelley-Hoskins[9], M. Kertzman[22], D. Kieda[21], M. Krause[9], F. Krennrich[13], S. Kumar[18], M. J. Lang[11], G. Maier[9], S. McArthur[12], A. McCann[1], K. Meagher[23], P. Moriarty[11], R. Mukherjee[14], T. Nguyen[23], D. Nieto[19], A. O'Faoláin de Bhróithe[9], R. A. Ong[6], A. N. Otte[23], N. Park[24], J. S. Perkins[25], A. Pichel[26], M. Pohl[8,9], A. Popkow[6], E. Pueschel[4], J. Quinn[4], K. Ragan[1], P. T. Reynolds[27], G. T. Richards[23], E. Roache[3], A. C. Rovero[26], M. Santander[14], G. H. Sembroski[12], K. Shahinyan[16], A. W. Smith[28], D. Staszak[1], I. Telezhinsky[8,9], J. V. Tucci[12], J. Tyler[1], S. Vincent[9], S. P. Wakely[24], O. M. Weiner[19], A. Weinstein[13], D. A. Williams[5], B. Zitzer[7]
(the VERITAS collaboration),
M. Fumagalli[29], and J. X. Prochaska[30]
[1] Physics Department, McGill University, Montreal, QC H3A 2T8, Canada
[2] Department of Physics, Washington University, St. Louis, MO 63130, USA
[3] Fred Lawrence Whipple Observatory, Harvard-Smithsonian Center for Astrophysics, Amado, AZ 85645, USA; wystan.benbow@cfa.harvard.edu, matteo.cerruti@lpnhe.in2p3.fr
[4] School of Physics, University College Dublin, Belfield, Dublin 4, Ireland
[5] Santa Cruz Institute for Particle Physics and Department of Physics, University of California, Santa Cruz, CA 95064, USA; caajohns@ucsc.edu
[6] Department of Physics and Astronomy, University of California, Los Angeles, CA 90095, USA
[7] Argonne National Laboratory, 9700 S. Cass Avenue, Argonne, IL 60439, USA
[8] Institute of Physics and Astronomy, University of Potsdam, D-14476 Potsdam-Golm, Germany
[9] DESY, Platanenallee 6, D-15738 Zeuthen, Germany
[10] Astronomy Department, Adler Planetarium and Astronomy Museum, Chicago, IL 60605, USA
[11] School of Physics, National University of Ireland Galway, University Road, Galway, Ireland
[12] Department of Physics and Astronomy, Purdue University, West Lafayette, IN 47907, USA
[13] Department of Physics and Astronomy, Iowa State University, Ames, IA 50011, USA
[14] Department of Physics and Astronomy, Barnard College, Columbia University, NY 10027, USA
[15] Department of Astronomy and Astrophysics, 525 Davey Lab, Pennsylvania State University, University Park, PA 16802, USA
[16] School of Physics and Astronomy, University of Minnesota, Minneapolis, MN 55455, USA
[17] Department of Physics, California State University—East Bay, Hayward, CA 94542, USA
[18] Department of Physics and Astronomy and the Bartol Research Institute, University of Delaware, Newark, DE 19716, USA
[19] Physics Department, Columbia University, New York, NY 10027, USA
[20] Department of Physics and Astronomy, University of Iowa, Van Allen Hall, Iowa City, IA 52242, USA
[21] Department of Physics and Astronomy, University of Utah, Salt Lake City, UT 84112, USA
[22] Department of Physics and Astronomy, DePauw University, Greencastle, IN 46135-0037, USA
[23] School of Physics and Center for Relativistic Astrophysics, Georgia Institute of Technology, 837 State Street NW, Atlanta, GA 30332-0430, USA
[24] Enrico Fermi Institute, University of Chicago, Chicago, IL 60637, USA
[25] N.A.S.A./Goddard Space-Flight Center, Code 661, Greenbelt, MD 20771, USA
[26] Instituto de Astronomia y Fisica del Espacio, Casilla de Correo 67—Sucursal 28, (C1428ZAA) Ciudad Autónoma de Buenos Aires, Argentina
[27] Department of Physical Sciences, Cork Institute of Technology, Bishopstown, Cork, Ireland
[28] University of Maryland, College Park/NASA GSFC, College Park, MD 20742, USA
[29] Institute for Computational Cosmology and Centre for Extragalactic Astronomy, Department of Physics, Durham University, South Road, Durham, DH1 3LE, UK
[30] Department of Astronomy and Astrophysics, University of California, Santa Cruz, CA 95064, USA
Received 2016 January 16; accepted 2016 March 7; published 2016 May 18

ABSTRACT

Between the beginning of its full-scale scientific operations in 2007 and 2012, the VERITAS Cherenkov telescope array observed more than 130 blazars; of these, 26 were detected as very-high-energy (VHE; $E > 100$ GeV) γ-ray sources. In this work, we present the analysis results of a sample of 114 undetected objects. The observations constitute a total live-time of ~570 hr. The sample includes several unidentified *Fermi*-Large Area Telescope (LAT) sources (located at high Galactic latitude) as well as all the sources from the second *Fermi*-LAT catalog that are contained within the field of view of the VERITAS observations. We have also performed optical spectroscopy measurements in order to estimate the redshift of some of these blazars that do not have spectroscopic distance estimates. We present new optical spectra from the Kast instrument on the Shane telescope at the Lick observatory for 18 blazars included in this work, which allowed for the successful measurement or constraint on the redshift of four of them. For each of the blazars included in our sample, we provide the flux upper limit in the VERITAS energy band. We also study the properties of the significance distributions and we present the result of a stacked analysis of the data set, which shows a 4σ excess.

[31] Now at Sorbonne Universités, UPMC Université Paris 06, Université Paris Diderot, Sorbonne Paris Cité, CNRS, Laboratoire de Physique Nucléaire et de Hautes Energies (LPNHE), 4 place Jussieu, F-75252, Paris Cedex 5, France.

Key words: BL Lacertae objects: general – galaxies: active – gamma rays: galaxies – radiation mechanisms: non-thermal

Supporting material: figure set

1. INTRODUCTION

The current generation of imaging atmospheric Cherenkov telescopes (IACTs), sensitive to very-high-energy (VHE; $E > 100\,\mathrm{GeV}$) γ-ray photons, has significantly increased our knowledge of blazars. They represent the class of objects that dominates the VHE extragalactic sky. Among the 66 extragalactic VHE sources currently detected,[32] about 90% of them are blazars.

In the framework of the unified model of active galactic nuclei (AGNs), blazars are radio-loud AGNs, characterized by a pair of relativistic jets of plasma emitted along the polar axis of the super-massive black-hole powering the system, aligned along the line of sight of the observer (see Urry & Padovani 1995). The observational properties of blazars include a spectral energy distribution (SED) characterized by a non-thermal continuum from radio to γ-rays, extreme temporal variability, and strong polarization. These properties can be explained by considering that the emission from the jet, enhanced by relativistic effects, dominates the SED (Angel & Stockman 1980). Spectroscopic measurements in optical and UV reveal that two distinct sub-classes of blazars exist: BL Lac objects, characterized by a featureless optical/UV spectrum, and flat-spectrum radio-quasars (FSRQs), which show instead broad emission lines. The traditional division between the two classes of objects is an equivalent width of the emission lines equal to 5 Å (see Stickel et al. 1991). The two sub-classes are also characterized by different luminosity and redshift distributions. The FSRQs are, on average, brighter and located at higher redshifts (see, e.g., Padovani 1992; Massaro et al. 2009). In the unified AGN model, this dichotomy is associated with a similar dichotomy seen in radio galaxies. FSRQs are considered the blazar version of FR II radio galaxies (Fanaroff & Riley 1974), while BL Lac objects correspond to FR I (Urry & Padovani 1995).

Two broad non-thermal components characterize blazar SEDs. The first, peaking between millimeter and X-rays, is attributed to synchrotron emission by a population of electrons/positrons in the blazar jet. The second, peaking in γ-rays, is associated, in leptonic models, with inverse-Compton scattering between the same leptons and their own synchrotron emission (synchtron-self-Compton model, SSC, Konigl 1981), or an external photon field, such as the emission from the dusty torus, the accretion disk or the broad-line region (see Sikora et al. 1994). Alternatively, in hadronic scenarios, the second SED component is attributed to synchrotron emission by protons, or by secondary particles produced in p–γ interactions (Mücke & Protheroe 2001). The position of the first peak is used to further classify BL Lac objects into low- and high-frequency-peaked BL Lac objects (LBL/HBL), depending on whether the peak frequency is located in infrared/optical or UV/X-rays, respectively. The transition between LBL and HBL is smooth, and a population of intermediate-frequency-peaked BL Lac objects exists as well (IBL, with $10^{14}\,\mathrm{Hz} < \nu_{\mathrm{syn}} < 10^{15}\,\mathrm{Hz}$, see Laurent-Muehleisen et al. 1998). While BL Lac objects present a variety of synchrotron peak frequencies, FSRQs are almost all characterized by a low-frequency peak. This classification can be seen as a more recent version of the older classification (see, e.g., Padovani & Giommi 1995b) of blazars into radio-selected objects (RBLs, which are more likely FSRQs and LBLs) and X-ray-selected objects (XBLs, which are more likely HBLs).[33]

The measurement of blazar spectral properties at VHE is important not only to characterize the blazar emission itself, but also to indirectly study the extragalactic background-light (EBL) in the infrared and visible bands due to the absorption that it causes on VHE photons via $e^{\pm}$ pair-production, (see Salamon & Stecker 1998). VHE observations can also be used to put limits on the strength of the intergalactic magnetic field according to the non-detection of the emission from the cascade triggered by the interaction of the pairs with the cosmic microwave background (see, e.g., Taylor et al. 2011).

Even though the detection and the measurement of the VHE spectrum of a blazar is of paramount importance for the comprehension of the physics of relativistic jets in AGNs and for cosmological studies, a non-detection in the VHE regime can also be extremely useful. It can constrain the source emission model, especially when the flux upper-limit is significantly lower than the extrapolation of the *Fermi*-Large Area Telescope (LAT; Atwood et al. 2009) measurement in high-energy γ-rays (HE; $100\,\mathrm{MeV} < E < 100\,\mathrm{GeV}$) up to VHE, implying the presence of a spectral cut-off. It can also constrain the variability properties of the source at VHE if the blazar has been previously detected or is detected at a later time during a higher flux state. Additionally, for the upcoming Cherenkov Telescope Array (CTA, Actis et al. 2011), it will be useful to have the information from all past observations performed by the current generation of IACTs, in order to make predictions for expected outcomes (see, e.g., Sol et al. 2013).

All three major IACTs (H.E.S.S., MAGIC, and VERITAS) have published upper limits on blazar VHE emission, including more than 70 sources in their lists (Aharonian et al. 2005, 2008b; Aleksić et al. 2011a; Aliu et al. 2012; Abramowski et al. 2014). Past IACTs, such as CAT, HEGRA, and Whipple, have also presented the results from undetected blazars (Piron 2000; Aharonian et al. 2004; Falcone et al. 2004; Horan et al. 2004), though, in general, their limits have been superseded by the current instruments. At higher energies, upper limits on blazars have also been estimated using the air-shower technique with Milagro (Williams 2005).

The study of blazars is complicated by the uncertainty in their redshifts. In fact, the almost featureless spectra of BL Lac objects imply that a redshift estimate can be obtained only via absorption features from the host galaxy or clouds in the intergalactic medium, or via molecular emission lines (see Fumagalli et al. 2012), or via a less precise photometric estimate (comparing the luminosity of the host galaxy to

[32] For a recent review, see, e.g., Şentürk et al. (2013); for an updated list of known VHE sources see http://tevcat.uchicago.edu.

[33] The classification of BL Lac objects as LBL/IBL/HBL is sometimes replaced by LSP/ISP/HSP (low/intermediate/high-synchrotron-peaked blazars, see Abdo et al. 2010b), making an explicit reference to the synchrotron origin of the first component of the SED. For BL Lac objects, the two triplets of acronyms can be considered as synonyms.

Table 1
List of Sources Observed by VERITAS

Source Name	R.A. (h m s)	Decl. (° m s)	z[a]	Type[b]	Exposure (hr)	$\hat{\theta}_{\rm zenith}$ (degree)	MJDs (−50000)	Selection[c]
RBS 0042	00 18 27.8	+29 47 32	0.100: (1)	HBL	7.1	15	4731/32/33/40 4741/42/46/73 5089/90/91 5131/43	SHBL
RBS 0082	00 35 14.7	+15 15 04	1.28: (2)	HBL	6.3	19	5100/01/02 5119/20/29/30	SHBL
1ES 0037+405	00 40 13.8	+40 50 05	-	HBL	36.0	14	4767/68/71/72 4773/89/91 4800/02/22/29/46 5156/57/58/59 5457/70/71/72 5475/76/77/78/79 5495/96/97/98 5500/01/23/26 5546/54/56	ToO
1RXS J0045.3+2127	00 45 19.2	+21 27 43	-	HBL	1.2	22	5512	N06, 1FGL
RGB J0110+418	01 10 04.9	+41 49 51	0.096 (3)	IBL (38)	4.0	13	4832/33 5866/67/68/96	P00
1ES 0120+340	01 23 08.7	+34 20 51	0.272 (4)	HBL	5.9	16	4383/84/93/94 4414/37/5171 5470/73/99 5512/26	SHBL, CG02
QSO 0133+476	01 36 58.6	+47 51 29	0.859 (5)	FSRQ (39)	0.8	40	4508	ToO
B2 0200+30	02 03 45.6	+30 41 30	0.761 (6)	-	1.8	21	5569/70/88	ToO
CGRaBS J0211+1051	02 11 13.1	+10 51 35	0.20: (7)	LBL (40)	4.0	31	5588/89/90/91 5595/99	ToO
RGB J0214+517	02 14 17.9	+51 44 52	0.049 (8)	IBL (41)	5.1	22	4773/89/90/91/94 4800/5156/81 5201/04/5489	P00, CG02
RBS 0298	02 16 30.9	+23 15 13	0.289 (9)	HBL	3.1	14	4731/32/33/73	SHBL
RBS 0319	02 27 16.6	+02 02 00	0.457 (10)	HBL	0.3	31	4412	SHBL
AO 0235+16	02 38 38.9	+16 36 59	0.94 (11)	LBL (41)	4.3	21	4737/38/39/42/45	1FGL, ToO
RGB J0250+172	02 50 38.0	+17 12 08	0.243 (12)	IBL (38)	5.1	22	5144/59/5472 5528/42/71/98	1FGL
2FGL J0312.8+2013	03 12 23.0	+20 07 50	-	-	9.7	14	5209 5830/33/34/40 5855/56/57/58 5860/61/62	2FGL
RGB J0314+247	03 14 02.7	+24 44 33	0.056 (3)	LBL (42)	3.1	28	4441 4761/62/63/64/73	P00
RGB J0314+063	03 14 23.9	+06 19 57	-	HBL	0.3	26	5868	SHBL
RGB J0321+236	03 22 00.0	+23 36 11	-	IBL (38)	9.2	12	5501/02/03/04 5507/08/10/11 5512/13/14	1FGL
B2 0321+33	03 24 41.2	+34 10 46	0.061 (8)	FSRQ/ NLS1 (43)	9.1	12	4409/12/16/37 4438/39/40/47 4448/49/50/64	P00, F04

Table 1
(Continued)

Source Name	R.A. (h m s)	Decl. (° m s)	z[a]	Type[b]	Exposure (hr)	$\hat{\theta}_{\rm zenith}$ (degree)	MJDs (−50000)	Selection[c]
1FGL J0333.7+2919	03 33 49.2	+29 16 32	-	IBL (44)	0.6	3	5571	1FGL
1RXS J044127.8+150455	04 41 27.4	+15 04 56	0.109 (13)	HBL	10.1	21	4747/48/49/89/90 4831/32/33 4847/49/51/79 4880/82/91	SHBL
2FGL J0423.3+5612	04 23 27.0	+56 12 24	-	-	1.6	28	5855/5926	2FGL
1FGL J0423.8+4148	04 23 56.1	+41 50 03	-	-	1.0	15	5599	1FGL
1ES 0446+449	04 50 07.3	+45 03 12	0.203: (4)	IBL (38)	7.1	22	4734/42/61/62 4763/64/65 5209/13/34/35 5838	S96
RGB J0505+612	05 05 58.7	+61 13 36	-	-	9.2	32	5502/03/29/30 5535/36/40/41 5543/44/57/58/72	1FGL
1FGL J0515.9+1528	05 15 47.3	+15 27 17	-	-	3.9	18	5480/81/82 5558/59	1FGL
2FGL J0540.4+5822	05 40 26.0	+58 22 54	-	-	1.3	30	5856/5926/27	2FGL
RGB J0643+422	06 43 26.8	+42 14 19	0.080 (14)	HBL	1.2	23	4439/4790/4892	B97
RGB J0656+426	06 56 10.7	+42 37 02	0.061 (15)	IBL (37)	9.4	16	4746/66/67/77 4778/79/90/4800	P00
1ES 0735+178	07 38 07.4	+17 42 19	0.424 (16)	IBL (44)	5.2	18	5531/32/58/59 5574/87/5602	1FGL
BZB J0809+3455	08 09 38.9	+34 55 37	0.082 (8)	HBL	1.6	13	5928/29/30	1FGL
PKS 0829+046	08 31 48.9	+04 29 39	0.174 (17)	IBL (37)	2.4	30	4822/4921/5181	M01
Mrk 1218	08 38 10.9	+24 53 43	0.028 (18)	FSRQ/ Sy1 (45)	5.9	13	4423/25/39/40 4448/49/50/52	F04
OJ 287	08 54 48.9	+20 06 31	0.306 (19)	LBL (46)	10.2	19	4438/39/40/48 4449/50/52/65/66 5233/35/37/66 5302	CG02, M01 ToO
B2 0912+29	09 15 52.4	+29 33 24	0.36: (7)	HBL	11.7	10	5571/72/74/75 5576/87/88/89/90 5630/44/72/73	1FGL
1ES 0927+500	09 30 37.6	+49 50 26	0.188 (4)	HBL	11.7	23	4466/4770/71 4800/01/02/03/06 4807/20/21/22 5247/75	SHBL, ROXA
RBS 0831	10 08 11.4	+47 05 22	0.343 (20)	HBL	1.6	18	5531/59/89	SHBL, ROXA
RGB J1012+424	10 12 44.3	+42 29 57	0.36: (21)	IBL (37)	1.7	15	5589/5931/86	ROXA
1ES 1028+511	10 31 18.5	+50 53 36	0.36: (10)	HBL	24.1	23	4412/13/15/4530 4828/29/30/31 4832/59/83 4905/06/11/21 4922/23/27/28 5292/93/95/98 5301/03	SHBL, CG02 ROXA

Table 1
(Continued)

Source Name	R.A. (h m s)	Decl. (° m s)	z[a]	Type[b]	Exposure (hr)	$\hat{\theta}_{\rm zenith}$ (degree)	MJDs (−50000)	Selection[c]
							5919/23/27/31/45 5946/58/70/79/82 6000/02/09/27 6035/38	
RGB J1037+571	10 37 44.3	+57 11 56	>0.62: (7)	IBL (37)	3.7	26	5241/42/43/46	1FGL
RGB J1053+494	10 53 44.1	+49 29 56	0.140 (22)	HBL	7.8	24	4879/81/82/88/91 4921/22 5157/58/59	1FGL
RBS 0921	10 56 06.6	+02 52 14	0.236 (23)	HBL	2.7	30	4821/22/51	SHBL
RBS 0929	11 00 21.1	+40 19 28	-	HBL	4.4	16	5333/5587/88/89	SHBL, ROXA
1ES 1106+244	11 09 16.2	+24 11 20	0.482 (24)	HBL	1.0	17	5981/82	C07
RX J1117.1+2014	11 17 06.3	+20 14 07	0.139 (15)	HBL	9.1	16	4940/41/42/5538 5540/41/42/43/44 5543/63/64/65/71	SHBL, CG02 1FGL, ToO
1ES 1118+424	11 20 48.1	+42 12 12	0.230 (12)	HBL	6.4	17	5212/32/74/75 5276/89/90/91	SHBL, S96
S4 1150+497	11 53 24.5	+49 31 09	0.334 (25)	FSRQ (38)	3.8	24	5701/02/03/04/05 5706/07/08/09/10	ROXA, ToO
RGB J1231+287	12 31 43.6	+28 47 50	1.03 (26)	HBL	5.1	17	5239/66/91/98 5300/03	1FGL
1ES 1239+069	12 41 48.3	+06 36 01	0.150 (4)	HBL	1.9	26	4979/80	S96
PG 1246+586	12 48 18.8	+58 20 29	>0.73: (10)	IBL (37)	9.6	29	5595/ 5601/03/05 5621/24/25/29 5630/31	1FGL
1ES 1255+244	12 57 31.9	+24 12 40	0.141 (27)	HBL	26.0	16	4531/34/68/80 4581/82/83/84 4585/86/87/91 4907/11/23/50 4970/79/80 5207/08/36 5591/5617 5947/49/53/59 5972/78/89 6016/42/44/45 6072/73/74	SHBL, S96
BZB J1309+4305	13 09 25.5	+43 05 06	0.691 (6)	HBL	9.4	15	5594/96/98 5600/02/04/06 5620/22/23/25	1FGL
1FGL J1323.1+2942	13 23 02.4	+29 41 35	-	FSRQ (47)	8.4	14	4832/34/92/93 4909/14/79 5596/97/99 5602/05/48/49	1FGL, ToO
RX J1326.2+2933	13 26 15.0	+29 33 31	0.431 (14)	HBL	8.4	14	Same as above	ROXA, C07
RGB J1341+399	13 41 05.2	+39 59 46	0.169 (14)	HBL	2.7	26	4938/78 5972/6045	ROXA, N06
RGB J1351+112	13 51 20.8	+11 14 53	>0.619 (28)	HBL	6.2	24	5210/21/39/40 5241/43/46	1FGL

Table 1
(Continued)

Source Name	R.A. (h m s)	Decl. (° m s)	z[a]	Type[b]	Exposure (hr)	$\hat{\theta}_{\rm zenith}$ (degree)	MJDs (−50000)	Selection[c]
							5293/97/98	
RX J1353.4+5601	13 53 28.1	+53 00 57	0.370 (14)	HBL	2.5	26	5589/90/6002	ROXA, N06
RBS 1350	14 06 59.2	+16 42 06	>0.623 (13)	HBL	4.5	22	5269/97/98 5300/01	1FGL
RBS 1366	14 17 56.7	+25 43 56	0.237 (12)	HBL	10.0	17	4591/92/93/94 4596/99 4611/12/13/15/16 6046	SHBL, CG02 ROXA
1ES 1421+582	14 22 38.9	+58 01 56	0.683 (14)	HBL	3.4	28	5324/25/26/28/30 5333/35/50/51	SHBL
RGB J1439+395	14 39 17.5	+39 32 43	0.344 (13)	HBL	1.5	12	5620/6002	SHBL, ROXA
1RXS J144053.2+061013	14 40 52.9	+06 10 16	0.396 (28)	IBL (48)	2.5	27	5731/32/34/35/36	1FGL
RBS 1452	15 01 01.8	+22 38 06	0.235 (29)	IBL (49)	4.1	21	5297/98/99	1FGL
RGB J1532+302	15 32 02.3	+30 16 29	0.065 (3)	HBL	6.5	17	4939/40/67/68 4970/75/76/77	P00
RGB J1533+189	15 33 11.3	+18 54 29	0.305 (13)	HBL	2.9	20	5648/77 5705/06/20	SHBL, ROXA N06
1ES 1533+535	15 35 00.9	+53 20 37	0.89: (10)	HBL	1.0	23	4256/6002	SHBL
RGB J1610+671B	16 10 04.1	+67 10 26	0.067 (14)	HBL	6.6	36	4908/38/5268 5292/93/94/95	P00
1ES 1627+402	16 29 01.3	+40 08 00	0.272 (3)	HBL/ NLS1 (50), (51)	13.1	16	4229/35/36 4537/38/39/40/57 4559/60/61/62/63 4564/65/69/83 4954	P02, F04
GB6 J1700+6830	17 00 09.3	+68 30 07	0.301 (30)	FSRQ (30)	0.8	37	4914/16	1FGL, ToO
PKS 1717+177	17 19 13.0	+17 45 06	>0.58 (31)	LBL (52)	5.1	18	4909/11/17/18 4920/21/22	1FGL
PKS 1725+045	17 28 25.0	+04 27 05	0.2966 (32)	FSRQ (53)	0.3	27	4412	M01
PKS 1749+096	17 51 32.8	+09 39 01	0.32 (33)	LBL (54)	0.3	22	6072	ToO
RGB J1838+480	18 39 49.2	+48 02 34	0.30: (21)	IBL (37)	0.5	26	6090	2FGL
RGB J1903+556	19 03 11.6	+55 40 39	>0.58: (7)	IBL (41)	1.0	27	5099	1FGL
1FGL J1926.8+6153	19 26 41.9	+61 54 41	-	-	1.3	31	5706/07	1FGL
PKS 2233-148	22 36 34.1	-14 33 22	>0.49: (34)	LBL (55)	0.3	49	6100	ToO
3C 454.3	22 53 57.7	+16 08 54	0.859 (35)	FSRQ (56)	1.0	24	5504/31	ToO
RGB J2322+346	23 22 44.0	+34 36 14	0.098 (3)	IBL (37)	2.9	10	4731/36/39 4745/46/47	P00
1ES 2321+419	23 23 52.1	+42 10 59	>0.45 (36)	HBL	4.2	21	4773/76 4802/03/30/31 5091	S96
B3 2322+396	23 25 17.9	+39 57 37	>1.05 (32)	LBL (54)	1.0	16	5118/30	1FGL
1FGL J2329.2+3755	23 29 14.2	+37 54 15	-	-	3.3	11	5470/71/72/75/76	1FGL

Table 1
(Continued)

Source Name	R.A. (h m s)	Decl. (° m s)	z[a]	Type[b]	Exposure (hr)	$\hat{\theta}_{\rm zenith}$ (degree)	MJDs (−50000)	Selection[c]
							5477/78/80	
1RXS J234332.5+343957	23 43 33.8	+34 40 04	0.366 (13)	HBL	1.5	17	5912	SHBL

Notes.
[a] Unconstrained redshifts are indicated with a hyphen (-). If the redshift value is uncertain, it is followed by a colon (:). Redshift references: (1) Fischer et al. (1998), (2) Rau et al. (2012), (3) Laurent-Muehleisen et al. (1998), (4) Perlman et al. (1996), (5) Lawrence et al. (1986), (6) Shaw et al. (2013), (7) Meisner & Romani (2010), (8) Marcha et al. (1996), (9) Böhringer et al. (2000), (10) Sbarufatti et al. (2005), (11) Cohen et al. (1987), (12) this work, (13) Piranomonte et al. (2007), (14) Bauer et al. (2000), (15) Lavaux & Hudson (2011), (16) Carswell et al. (1974), (17) Falomo (1991), (18) Osterbrock & Dahari (1983), (19) Stickel et al. (1989), (20) Plotkin et al. (2010), (21) Nilsson et al. (2003), (22) Stocke et al. (1991), (23) Cao et al. (1999), (24) Sbarufatti et al. (2009), (25) Burbidge et al. (1977), (26) White et al. (2000), (27) Padovani & Giommi (1995a), (28) Sandrinelli et al. (2013), (29) Jannuzi et al. (1993), (30) Henstock et al. (1997), (31) Shaw et al. (2009), (32) Eracleous & Halpern (2004), (33) Stickel et al. (1988), (34) Sbarufatti et al. (2006), (35) Smith et al. (1976), (36) Falomo & Kotilainen (1999).
[b] Blazars of unknown type are indicated with a hyphen (-). Blazar type references: (37) Laurent-Muehleisen et al. (1999), (38) Giommi et al. (2012), (39) Chandra et al. (2012), (40) Ackermann et al. (2012b), (41) Nieppola et al. (2006), (42) Abdo et al. (2009b), (43) Massaro et al. (2012), (44) Rani et al. (2011), (45) Osterbrock & Dahari (1983), (46)Impey & Neugebauer (1988), (47) Cornwell et al. (1986), (48) Ajello et al. (2014), (49) Massaro et al. (2003), (50) Padovani et al. (2002), (51) Komossa et al. (2006), (52) Li et al. (2010), (53) Drinkwater et al. (1997), (54) Abdo et al. (2010b), (55) Lister et al. (2011), (56) Smith et al. (1976).
[c] Source selection references: *1FGL*, Abdo et al. (2010a); *2FGL*, Nolan et al. (2012); *B97*, Brinkmann et al. (1997); *CG02*, Costamante & Ghisellini (2002); *C07*, Costamante (2007); *F04*, Falcone et al. (2004); *M01*, Mukherjee (2001); *N06*, Nieppola et al. (2006); *ROXA*, Turriziani et al. (2007); *S96*, Stecker et al. (1996); *SHBL*, Giommi et al. (2005); *P00*, Perlman (2000); *P02*, Padovani et al. (2002); *ToO*, Target of Opportunity.

samples of giant elliptical galaxies). If the blazar belongs to a group of galaxies, its redshift can also be estimated by studying the non-active companions (see Muriel et al. 2015). For VHE studies, the knowledge of the redshift of the blazar is very important, because the absorption by the EBL increases with the distance of the object. Currently, the farthest detected VHE blazar is the gravitationally lensed quasar S3 0218+357 (Mirzoyan 2014b) at $z = 0.944$, closely followed by the FSRQ PKS 1441+25 (Abeysekara et al. 2015; Ahnen et al. 2015) at $z = 0.939$, while the farthest, persistent (i.e., detected not only during episodic flaring activity) VHE blazar is PKS 1424+240 ($z > 0.61$, see Acciari et al. 2010; Furniss et al. 2013; Archambault et al. 2014). To improve the constraints on the distance of some VHE candidates, new redshift estimates obtained with the Kast spectrograph at the Lick Observatory (see Section 2 and the Appendix) are presented together with the VHE upper limits from VERITAS.

In this paper, we present the results of the analysis of most of the non-detected blazars observed by VERITAS from 2007 (the beginning of full-scale scientific operations) to 2012 August (before the upgrade of the VERITAS array, see Kieda 2013). VERITAS upper limits on six VHE candidates were presented by Aliu et al. (2012). The sample also includes several unidentified *Fermi*-LAT objects (located at high Galactic latitude, and most likely associated with unidentified AGNs, see Ackermann et al. 2012a; Mirabal et al. 2012; Doert & Errando 2014).

The paper is organized as follows. In Section 2, we provide the details of the properties of the sample and the source selection. The details of the VERITAS data analysis and results are provided in Section 3. A stacked analysis of the data is presented in Section 4, studying the full data set as well as sub-data sets defined by redshifts and blazar classes. The conclusions are in Section 5.

2. THE SAMPLE AND NEW REDSHIFT ESTIMATES

Blazars targeted by VERITAS as VHE source candidates were selected according to a variety of criteria. Early source selections were based on blazar X-ray or radio catalogs, while more recent candidates have also been selected on the basis of their *Fermi*-LAT spectral characteristics (Abdo et al. 2009a, 2010a; Nolan et al. 2012) or on their association with clusters of HE γ-rays (see Archambault et al. 2013). The target list includes the following.

1. All the nearby ($z < 0.3$) HBL/IBL recommended as potential VHE emitters by Stecker et al. (1996), Perlman (2000), and Costamante & Ghisellini (2002).
2. The X-ray brightest nearby ($z < 0.3$) HBL in the Sedentary (Giommi et al. 2005) and ROXA (Turriziani et al. 2007) surveys.
3. Four distant ($z > 0.3$) BL Lac objects recommended by Costamante & Ghisellini (2002) and Costamante (2007).
4. All nearby ($z < 0.3$) blazars detected by *EGRET* (Mukherjee 2001).
5. Several FSRQs recommended as potential VHE emitters by Perlman (2000) and Padovani et al. (2002).
6. Two high-frequency-peaked FSRQs (B2 0321+33 and Mrk 1218, see Perlman 2000; Falcone et al. 2004), which have also been classified as Seyfert-1 galaxies (see Osterbrock & Dahari 1983; Abdo et al. 2009b).
7. The brightest *Fermi*-LAT sources after extrapolation into the VERITAS energy band (Abdo et al. 2009a, 2010a; Nolan et al. 2012).
8. Sources associated with clusters of HE γ-rays, but not included in *Fermi*-LAT catalogs, similar to *VERJ0521+211* (Archambault et al. 2013).

In addition, several targets have been observed by VERITAS only as targets of opportunity (ToO), following flare alerts by multi-wavelength partners (see Errando 2011).

The sources included in our sample are listed in Table 1 (for sources without VHE detection, 82 targets) and Table 2 (for known VHE emitters, detected by other instruments, or by VERITAS after 2012 and during flaring activity, 11 targets). Sources are listed in order of increasing Right Ascension (R.A.). For every target, we indicate the name, the coordinates (R.A. and decl., in J2000), the catalog redshift z, the blazar class, the VERITAS dead-time corrected exposure (see Section 3), the average zenith angle of VERITAS observations,

Table 2
List of Known VHE Sources Observed but Not Detected by VERITAS in 2007–2012

Source Name	R.A. (h m s)	Decl. (° m s)	z[a]	Type	Exposure (hr)	$\hat{\theta}_{\rm zenith}$ (degree)	MJDs (−50000)	Selection[b]	VHE detection[c]
1ES 0033+595	00 35 52.6	+59 50 05	0.086: (1)	HBL	22.6	31	4411/18/19/20 4421/38/40/48 4464/66/76 4734/36/37/74 4775/76/77 4803/04/06 5866/67	CG02, P00	1
RGB J0152+017	01 52 33.5	+01 46 40	0.080 (2)	HBL	8.4	35	4421/22/37/38 4439/40/47/48 4449/50/64/65/78 5537/5832/33/68	CG02	2
RGB J0847+115	08 47 13.0	+11 33 50	0.198 (3)	HBL	12.1	25	4499/4505/07/08 4522/23/24/25/26 5303 5502/03/31/59	SHBL	3
RX J1136.5+6737	11 36 30.1	+67 37 04	0.134 (4)	HBL	7.7	37	4860/61/91/92 4918/21 5292/94/99 5303	CG02, SHBL ROXA	4
PKS 1222+216	12 24 54.4	+21 22 47	0.432 (5)	FSRQ	25.8	16	4939/5182 5318/19/20/21 5322/24/25/26 5327/28/30/33 5622/24/25/26 5631/33/34	ToO	5a, 5b
3C 279	12 56 11.1	-05 47 22	0.536 (6)	FSRQ	8.3	40	5623 5707/08/09/10 5711/15/17 5923/24/25/26/27 6016	ToO	6a, 6b
PKS 1510-089	15 12 52.2	-09 06 22	0.361 (7)	FSRQ	14.9	42	4909/11/48 5976/77/78/79 5980/81/82/83 5984/87	ToO	7a, 7b
RGB J1725+118	17 25 04.3	+11 52 16	>0.35: (8)	HBL	10.0	23	4593/94 4615/16/17/18 4619/20/21/22	CG02	8
0FGL J2001.0+4352	20 01 13.5	+43 53 03	0.18: (9)	HBL	4.9	25	5143/44/46/51/52 5326/52/57	1FGL	9
RGB J2243+203	22 43 54.7	+20 21 04	>0.39: (10)	IBL	4.1	17	5094/98/99 5101/16/28/29	1FGL	10
B3 2247+381	22 50 06.6	+38 25 58	0.118 (2)	HBL	6.0	13	5092/93/95/96/97 5832/89	1FGL	11

Notes.
[a] If the redshift value is uncertain it is followed by a colon (:). Redshift references: (1) private communication from Perlman, see Falomo & Kotilainen (1999), (2) Laurent-Muehleisen et al. (1998), (3) Cao et al. (1999), (4) Bade et al. (1994), (5) Burbidge & Kinman (1966), (6) Marziani et al. (1996), (7) Thompson et al. (1990), (8) Landoni et al. (2014), (9) Aleksić et al. (2014a), (10) Meisner & Romani (2010).
[b] Selection references: see Table 1.
[c] VHE detection references (see also for the blazar subclass classification): (1) Aleksić et al. (2015a), (2) Aharonian et al. (2008a), (3) Mirzoyan (2014c), (4) Mirzoyan (2014a), (5a) Aleksić et al. (2011b), (5b) Holder (2014a), (6a) Albert et al. (2008), (6b) Aleksić et al. (2014c), (7a) Abramowski et al. (2013a), (7b) Aleksić et al. (2014b), (8) Cortina (2013), (9) Aleksić et al. (2014a), (10) Holder (2014b), (11) Aleksić et al. (2012).

Table 3
List of 2FGL Sources in the VERITAS Field of View of Sources Listed in Tables 1 and 2

Source Name	Counterpart	R.A.[a] (h m s)	Decl.[a] (° m s)	z[b]	Type[c]	in FOV of[d]
2FGL J0047.9+2232	BWE 0045+2218	00 48 02.5	+22 34 53	1.161 (1)	FSRQ (12)	RGB J0045+214
2FGL J0148.6+0127	PMN J0148+0129	01 48 33.8	+01 29 01	0.940 (2)	-	RGB J0152+017
2FGL J0158.4+0107	-	01 58 25.4	+01 07 31	-	-	RGB J0152+017
2FGL J0205.4+3211	1Jy 0202+319	02 05 04.9	+32 12 30	1.466 (3)	FSRQ (13)	B2 0200+30
2FGL J0212.1+5318	-	02 12 09.4	+53 18 19	-	-	RGB J0214+517
2FGL J0213.1+2245	1RXS J021252.2+224510	02 12 52.8	+22 44 52	0.459 (2)	HBL (14)	RBS 0298
2FGL J0326.1+2226	TXS 0322+222	03 25 36.8	+22 24 00	2.06 (4)	FSRQ (15)	RGB J0321+236
2FGL J0440.4+1433	TXS 0437+145	04 40 21.1	+14 37 57	-	-	1RXS J044127.8+150455
2FGL J0856.3+2058	TXS 0853+211	08 56 39.7	+20 57 43	>0.388 (5)	-	OJ 287
2FGL J0929.5+5009	QSO J0929+5013	09 29 15.4	+50 13 36	0.370 (6)	IBL (16)	1ES 0927+500
2FGL J1058.4+0133	4C 01.28	10 58 29.6	+01 33 58	0.888 (7)	FSRQ (13)	RBS 0921
2FGL J1059.0+0222	PMN J1059+0225	10 59 06.0	+02 25 12	-	-	RBS 0921
2FGL J1141.0+6803	1RXS J114118.3+680433	11 41 18.0	+68 04 33	-	-	RX J1136.5+6737
2FGL J1239.5+0728	PKS 1236+077	12 38 24.6	+07 30 17	0.400 (8)	FSRQ (17)	1ES 1239+069
2FGL J1245.1+5708	GB6 J1245+5710	12 45 10.0	+57 09 54	>0.521 (5)	LBL (18)	PG 1246+586
2FGL J1303.1+2435	VIPS J13030+2433	13 03 03.2	+24 33 56	0.993 (9)	LBL (19)	1ES 1255+244
2FGL J1359.4+5541	VIPS J13590+5544	13 59 05.7	+55 44 29	1.014 (1)	FSRQ (12)	RX J1353.4+5601
2FGL J1722.7+1013	TXS 1720+102	17 22 44.6	+10 13 36	0.732 (10)	FSRQ (20)	RGB J1725+118
2FGL J1727.9+1220	PKS 1725+123	17 28 07.1	+12 15 39	0.583 (11)	FSRQ (20)	RGB J1725+118
2FGL J1927.5+6117	S4 1926+611	19 27 30.4	+61 17 33	-	LBL (21)	1FGL J1926.8+6153
2FGL J1959.9+4212	1RXS J195956.1+421339	19 59 56.1	+42 13 39	-	-	0FGL J2001.0+4352

Notes.
[a] Coordinates are provided for the counterpart. If the *Fermi*-LAT source is not associated with any lower-energy blazar, coordinates from the 2FGL catalog are given instead.
[b] Unconstrained redshifts are indicated with a hyphen (−). Redshift references: (1) Shaw et al. (2012), (2) Shaw et al. (2013), (3) Kraus & Gearhart (1975), (4) Halpern et al. (1986), (5) Plotkin et al. (2010), (6) Healey et al. (2008), (7) Hewitt & Burbidge (1993), (8) White et al. (1988), (9) Glikman et al. (2007), (10) Afanas'Ev et al. (2005), (11) Sowards-Emmerd et al. (2005).
[c] Blazars of unknown type are indicated with a hyphen (−). Blazar type references: (12) Shaw et al. (2012), (13) Kraus & Gearhart (1975), (14) Ajello et al. (2014), (15) Ghisellini et al. (2011), (16) Laurent-Muehleisen et al. (1999), (17) Hewitt & Burbidge (1993), (18) Plotkin et al. (2010), (19) Glikman et al. (2007), (20) Afanas'Ev et al. (2005), (21) Maselli et al. (2010).
[d] See Tables 1 and 2 for information on the exposure and the zenith angle of the observations.

the dates of VERITAS observations (in MJD) and on which basis the source was selected as a VHE candidate. Names and coordinates are taken from the *SIMBAD* database.[34] The references for the redshift estimates (and their uncertainties) and the blazar class are provided in the table notes. For every source, the archival SED from the *ASDC SED Builder* tool[35] has been visually inspected. It is used to classify all BL Lac objects marked as HBLs. The total number of hours of VERITAS data analyzed is about 570, which represents about 60% of a single VERITAS yearly observing season, i.e., about one-tenth of all good quality VERITAS data taken from 2007 to 2012.

The field of view (FOV) of the VERITAS telescope array is about 3°.5 and for every observation there is a chance that, in addition to the targeted blazar, other γ-ray sources are contained within the FOV. For every target included in our sample, we checked if other known γ-ray sources (included in the two-year *Fermi*-LAT catalog, 2FGL, see Nolan et al. 2012) were present in the FOV. Twenty-one 2FGL sources were indirectly observed by VERITAS through proximity to the blazar of interest, and are listed in Table 3. We also indicate the counterpart name (from the 2FGL catalog), the coordinates (R. A. and decl.) of the counterpart, the redshift, and the blazar sub-class (if known). The majority of these additional 2FGL sources are AGNs without classification.

[34] http://simbad.u-strasbg.fr/simbad/
[35] http://tools.asdc.asi.it/SED/

2.1. New Redshift Measurements

In order to measure the distance of some γ-ray blazars, we observed 18 of the VERITAS targets using the dual-arm Kast spectrograph at the Cassegrain focus of the Shane telescope at the Lick Observatory. For all the observations presented here, the instrument was configured with the 600/4310 grism on the blue arm, and the 600/7500 grating on the red arm, the D55 dichroic, and a 2″ slit. The dichroic crossover creates an instrumental gap located at ∼5500 Å and affects approximately 200 Å of the spectrum. In the spectroscopic Figures 2.1–2.6 (Appendix), this gap is shown on each spectrum. While the absolute fluxes are shown in the plots, the flux calibration is the least certain aspect of the spectra. In several spectra, there is a gap in flux across the dichroic; this is purely the result of calibrations and is not intrinsic to the AGN. The wavelength coverage is from ∼3450 to ∼8000 Å, but tellurics and fringing mask features above 6850 Å. We do not show this contaminated portion in the spectra. The targets, observation dates, and exposures are summarized in Table 7. The corresponding standard star and the signal-to-noise ratio (S/N) are also included in this table. The data were reduced following standard techniques with the Low-Redux pipeline.[36] Each spectrum was inspected visually for absorption or emission features. Features are noted in the spectral plots, Figures 2.1–2.6, and in Table 7. For 14 of the sources observed, there

[36] http://www.ucolick.org/~xavier/LowRedux/

are no spectral features that allow redshift measurements or redshift limits. By definition, BL Lac objects have no or weak spectral lines, so this high rate of non-detections is somewhat expected. Below are the sources for which features were found that allow for redshift determinations (see Figure 2):

1. RGB J0250+172.

   Observations of the source were obtained on 2010 August 15 (UT) and resulted in the detection of galactic features at $z = 0.243$. We detected Ca II (H, equivalent width (EW) $= 870 \pm 160$ mÅ; K, EW $= 1340 \pm 190$ mÅ), G-band (EW $= 650 \pm 180$ mÅ), and Mg I (EW $= 530 \pm 120$ mÅ) absorption. In the literature, Bauer et al. (2000) quotes a redshift of $z = 1.10$ for RGB J0250+172; however, there is no information on spectroscopic lines provided within the reference. Nilsson et al. (2003) present optical images of BL Lac objects, including RGB J0250+172. They find that the object is clearly resolved and state that $z = 1.10$ is too high because it results in a host galaxy that is exceedingly bright ($M_R < -29.0$). Based on fits to the observed light profile, a redshift estimate of $z = 0.25$ is provided, which is similar to the value measured within this work.
2. 1ES 1118+424.

   Observations of the source were obtained on 2013 February 14 (UT) and resulted in the detection of galactic features at $z = 0.230$. We detected Ca II (H, EW $= 11500 \pm 1500$ mÅ; K, EW $= 13000 \pm 1700$ mÅ), G-band (EW $= 3790 \pm 862$ mÅ), Ca I (EW $= 1208 \pm 199$ mÅ), and Mg I (EW $= 2896 \pm 254$ mÅ) absorption lines. In the literature, the redshift for 1ES 1118+424 is quoted as $z = 0.124$ from a private communication (see Falomo & Kotilainen 1999). However, Falomo & Kotilainen (1999) derive a lower limit of $z > 0.5$ based on images taken using the Nordic Optical Telescope, where the source is unresolved. They simulate an elliptical host galaxy with $M_R = -23.8$ and an effective radius of 10 kpc to determine the lowest redshift at which it would not be resolved. These galactic parameters are what they find from other BL Lac objects in their study, and they note that assuming a less luminous and smaller host galaxy would result in a lower redshift estimate.
3. RBS 1366 (=1E 1415+25.9).

   Observations of the sources obtained on 2014 May 30 (UT) resulted in the detection of galactic features at $z = 0.237$. We detected Ca II (H, EW $= 1300 \pm 130$ mÅ; K, EW $= 1570 \pm 140$ mÅ), G-band (EW $= 210 \pm 160$ mÅ), Ca I (EW $= 710 \pm 64$ mÅ), and Mg I (EW $= 1900 \pm 100$ mÅ) absorption.

   Halpern et al. (1986) also measure a redshift of $z = 0.237$ based on Ca II, G-band, Fe I, Mg I, and Na absorption. This source displays the significant variability associated with BL Lac objects. The spectrum taken in 2013 has a lower overall flux than the spectrum taken in 2014 (see Table 7), indicating that the source might have been in different flux states.
4. 1ES 2321+419.

   Observations of the source obtained on 2014 October 28 (UT) resulted in the detection of absorption features at $z = 0.267$. We detected Ca II (H, EW $= 260 \pm 47$ mÅ; K, EW $= 180 \pm 52$ mÅ) and Mg II (2796 Å, EW $= 740 \pm 83$ mÅ; 2803 Å, EW $= 510 \pm 67$ mÅ) absorption. Because the Ca II absorption is narrow, and there are no other galactic features, only a lower limit can be set on the redshift of the source. Additionally, there is potentially Mg II absorption at a higher redshift, $z = 0.346$. In the literature, Falomo & Kotilainen (1999) derive a lower limit for this source of $z > 0.45$ using the same technique as for 1ES 1118+424. While our value is not inconsistent, it is considerably lower than that placed based on assumptions about the host galaxy.

3. VERITAS OBSERVATIONS AND DATA ANALYSIS

The VERITAS (Very Energetic Radiation Imaging Telescope Array System) telescope array is composed of four IACTs of 12 m diameter each, located at the Fred Lawrence Whipple Observatory, on the slopes of Mount Hopkins, in southern Arizona (31°40′ N, 110° 57′ W). Each telescope has a segmented mirror that focuses light onto a camera composed of 499 photomultipliers located at the focal plane. The instrument FOV is 3.°5. For further details on the VERITAS instrument, see Holder et al. (2006) and Holder (2011).

The telescopes measure the faint Cherenkov light induced by the electromagnetic showers triggered by the interaction of the γ-ray photons with the Earth atmosphere. Similar cascades triggered by cosmic-rays are also detected by VERITAS, and can be rejected by applying specific cuts on the shape of the Cherenkov image (Hillas 1985).

The results presented in this paper have been obtained using a set of γ-hadron separation cuts specifically optimized for the detection of soft spectrum sources (differential spectrum parametrized by a power-law function $dN/dE = N(E/E_0)^{-\Gamma}$ with $\Gamma = 3.5$). The spectral index assumed is in line with the typical value of Γ observed for VHE blazars (see Şentürk et al. 2013).

All the observations presented in this paper were made using the *"wobble"* observing strategy (Fomin et al. 1994). Here, the telescopes point 0.°5 away from the target, alternatively in each of the four cardinal directions, to enable background estimation from the same FOV. This procedure ensures a similar acceptance for both the source (ON) and the background (OFF) regions. Regions overlapping bright stars are excluded from background estimates. The ratio of the ON over the OFF region size defines the background normalization parameter α. The dead time of the telescope array is explicitly calculated and is approximately 10% for the observations described here. The exposure values provided in Table 1 are all corrected for dead time, and represent the effective live-time of VERITAS observations.

The VERITAS observations here have an average length of 20 minutes (referred to as a *run*), before switching targets or wobble directions. For quality assurance, all the runs with a length lower than 10 minutes were excluded, often being associated with technical problems, resulting in the early termination of the run. Additionally, all observations characterized by non-optimal weather conditions or malfunctioning hardware were excluded from the run selection. On certain occasions, one of the VERITAS telescopes can be non-operational due to technical problems; all the runs analyzed in this paper have at least three telescopes in operation. Runs with all four telescopes in operation represent the bulk (92%) of the data.

In the standard configuration, VERITAS observations are not performed under bright-moonlight conditions (moon illumination >35% of full moon). Since 2012, the VERITAS

collaboration has started a new observing program in order to extend the duty cycle of the observatory and perform observations also under bright moonlight (Archambault et al. 2015). None of the data presented in this paper were taken under bright-moonlight conditions. Observations performed under moderate moonlight (moon illumination <35%) are included and analyzed in the same manner as dark-time observations, with appropriate instrument response functions to account for the increased night-sky background.

The significance at the source location is computed using Equation (17) in Li & Ma (1983). The upper limit on the VHE flux is estimated according to Rolke et al. (2005) at the 99% confidence level. It is first calculated assuming three different values of the spectral index ($\Gamma = 2.5$, 3.5 and 4.5) in order to estimate the decorrelation energy $E_{\rm dec}$ (the energy at which the upper limit estimate depends the least on the spectral index). The upper limit is then recomputed at the reference energy $E_{\rm dec}$ assuming a spectral index $\Gamma = 3.5$. The threshold of the analysis (which depends mainly on the zenith angle of the observations) is also calculated. For every source, we verified that, not only the overall significance is lower than five standard deviations (σ), but that no flares have been detected, i.e., that none of the sources was detected at more than 4σ during any single run.

For sources that are detected by *Fermi*-LAT (76% of the sample), the flux is extrapolated into the VERITAS energy band, taking into account the absorption from the EBL using the model by Franceschini et al. (2008), which is in agreement with the most recent observational constraints (Abramowski et al. 2013b). The extrapolated flux is then compared to the VERITAS upper limit. If the VERITAS measurement is lower than the extrapolation, it means that an additional cut-off should be present in the γ-ray component between the *Fermi*-LAT and the VERITAS energy bands.

The results of the analysis are reported in Tables 4 and 5 (for known VHE sources) and 6 (for 2FGL sources in the VERITAS FOV). For every target, we provide the significance, the number of ON and OFF counts, the value of the α parameter (ratio of the ON over OFF region size), the threshold of the analysis $E_{\rm th}$, the decorrelation energy $E_{\rm dec}$, the differential flux upper limit at $E_{\rm dec}$, the integral flux upper limit (above $E_{\rm th}$, provided in Crab units, following Hillas et al. 1998)[37], the ratio between the VERITAS differential upper limit and the extrapolation of the *Fermi*-LAT detection ($\Phi_{\rm HE}$, evaluated at $E_{\rm dec}$). Note that the values of the decorrelation and threshold energies are provided with three decimal values to ease any extrapolation to other energy bands, but they are known only to the second decimal value.

All the results presented in this paper have been cross-checked using a separate analysis, which provided consistent results for the single upper limit values, significance distributions (Section 3.2) and stacked analysis (Section 4).

[37] The best-fit of the VHE emission from the Crab Nebula as measured with the Whipple 10 m telescope and presented in Hillas et al. (1998) is a power-law function with index $\Gamma = 2.49$ and normalization $K = 3.2 \times 10^{-11}\,{\rm cm}^{-2}\,{\rm s}^{-1}\,{\rm TeV}^{-1}$ at 1 TeV. The integral upper limits are computed from the differential ones and provided here as a reference. They can easily be recomputed for different values of $E_{\rm th}$, or for other definitions of the Crab unit. For example, using as a reference the MAGIC spectrum of the Crab Nebula (Aleksić et al. 2015b), the Crab unit above 200 GeV is 74% of the Whipple Crab unit above the same threshold.

3.1. Notes on Individual Sources

Among the blazars targeted by VERITAS between 2007 and 2012, 11 of them were later identified as VHE emitters. They are listed in Table 2. The VERITAS upper limits are useful in these cases to constrain the properties of the VHE emission during low-flux states, as well as the variability properties of the source. The discussion of these blazar observations, in order of R.A., follows.

1. 1ES 0033+595 (HBL, $z = 0.086$:).
   VHE emission from 1ES 0033+595 was discovered by MAGIC (Aleksić et al. 2015a). The flux, measured from 24 hours of observations taken from 2009 August to October, is 0.9% Crab above 290 GeV.[38] The observed spectral index during the MAGIC observations is 3.8 ± 0.7. The VERITAS upper limit (5.4% Crab above 290 GeV) is fully consistent with the MAGIC measurement. The VHE variability of the source has been demonstrated by more recent VERITAS observations, which detected a bright VHE flare (with integral flux higher than 10% Crab) from the source during 2013 September, with simultaneous X-ray and ultraviolet coverage by *Swift* (Benbow 2015). A paper presenting the results of this multi-wavelength campaign is currently in preparation.
2. RGB J0152+017 (HBL, $z = 0.08$).
   This source has been known as a VHE emitter since 2008 (Aharonian et al. 2008a), when it was detected by H.E.S.S. at a flux of 2.6% Crab above 240 GeV, during 15 hr of observation. VERITAS observed the blazar in three different seasons: 2007–2008 (covering the H.E.S.S. period), 2010–2011, and 2011–2012. The VERITAS upper limit (3.6% Crab above 240 GeV) is fully consistent with the H.E.S.S. detection.
3. RGB J0847+115 (HBL, $z = 0.198$).
   VHE emission from this blazar was announced by MAGIC in 2014, at a flux corresponding to 2.5% Crab above 200 GeV (Mirzoyan 2014c). No spectral information is currently available, but the MAGIC collaboration reported a preliminary classification of the source as an extreme-HBL, with synchrotron peak frequency in hard-X-rays, and inverse-Compton peak frequency at TeV energies. Evidence of VHE and optical variability was also claimed by MAGIC. The VERITAS upper limit (2.0% of the Crab Nebula flux above 180 GeV) is marginally consistent with the preliminary flux estimate by MAGIC, and could be related to variability of the VHE emission.
4. RX J1136.5+6737 (HBL, $z = 0.134$).
   The MAGIC collaboration recently reported the detection of this source at a flux of 1.5% Crab above 200 GeV, in 20 hours of observations between 2014 January and April (Mirzoyan 2014a). No spectral information is available at the present time. The VERITAS upper limit (5.2% Crab above 290 GeV) is fully consistent with the preliminary flux estimate by MAGIC.

[38] In order to ease the comparison between the results from different instruments, the integral fluxes provided in this section have been recomputed above the VERITAS threshold, when the spectral information is available, and are expressed in Crab units as defined in Hillas et al. (1998).

Table 4
Analysis Results and Flux Upper Limits for the Non-detected AGNs Observed by VERITAS

Source Name	σ	ON	OFF	α	$E_{\rm th}$ (TeV)	$E_{\rm dec}$ (TeV)	$\mathrm{UL}_{@E_{\rm dec}}$ (10^{-12} cm^{-2} s^{-1} TeV^{-1})	$\mathrm{UL}_{>E_{\rm th}}$ (% C.U.)	$\mathrm{UL}/\Phi_{\rm HE}$
RBS 0042	0.02	1239	6455	0.192	0.182	0.345	8.7	2.2	0.2 ($z = 0.1$)
RBS 0082	0.16	1680	9062	0.185	0.166	0.264	16.9	1.8	45.0
1ES 0037+405	1.50	7515	64132	0.115	0.166	0.322	29.3	6.3	-
1RXS J0045.3+2127	2.04	224	1116	0.172	0.166	0.297	54.6	8.9	3.0/14.8 ($z = 0.1/0.5$)
RGB J0110+418	−0.02	801	4810	0.167	0.182	0.299	22.4	3.4	-
1ES 0120+340	1.47	1174	5215	0.214	0.166	0.283	24.6	3.4	1.4
QSO 0133+476	1.24	114	496	0.202	0.417	0.728	11.8	17.4	1.9e4
B2 0200+30	1.38	495	2775	0.167	0.151	0.273	51.9	6.9	59.6
CGRaBS J0211+1051	1.01	977	5659	0.167	0.200	0.318	20.8	3.6	3.4
RGB J0214+517	0.33	1113	5877	0.187	0.182	0.336	15.9	3.7	-
RBS 0298	1.76	606	3245	0.173	0.240	0.435	21.5	9.2	-
RBS 0319	−0.52	61	393	0.167	0.219	0.351	38.4	8.6	44.9
AO 0235+16	0.63	704	4116	0.167	0.182	0.311	18.7	3.2	9.6
RGB J0250+172	−0.06	1274	5637	0.226	0.166	0.316	13.5	2.7	1.4
2FGL J0312.8+2013	−0.36	2124	9046	0.238	0.166	0.257	10.0	1.0	0.5/0.6 ($z = 0.1/0.5$)
RGB J0314+247	1.07	691	3967	0.167	0.240	0.460	16.4	8.5	-
RGB J0314+063	1.18	76	326	0.200	0.182	0.294	76.7	11.0	-
RGB J0321+236	1.24	3065	17948	0.167	0.138	0.233	31.2	2.6	2.0/2.9 ($z = 0.1/0.5$)
B2 0321+33	−0.03	2190	8223	0.267	0.166	0.272	9.7	1.2	15.9
1FGL J0333.7+2919	0.37	158	606	0.223	0.138	0.226	101.0	7.6	2.7/7.4 ($z = 0.1/0.5$)
1RXS J044127.8+150455	1.83	2351	10636	0.212	0.182	0.338	17.5	4.1	-
2FGL J0423.3+5612	0.67	283	1522	0.178	0.240	0.457	16.4	8.3	1.9/32.6 ($z = 0.1/0.5$)
1FGL J0423.8+4148	−0.22	240	1462	0.167	0.166	0.274	46.4	5.7	0.6/2.2 ($z = 0.1/0.5$)
1ES 0446+449	−1.49	1482	10866	0.142	0.219	0.363	4.7	1.2	-
RGB J0505+612	−1.50	2167	9896	0.227	0.219	0.377	4.1	1.2	0.6/5.7 ($z = 0.1/0.5$)
1FGL J0515.9+1528	−0.54	1149	6734	0.173	0.151	0.283	16.7	2.5	0.9/3.8 ($z = 0.1/0.5$)
2FGL J0540.4+5822	0.43	226	1315	0.167	0.240	0.459	16.5	8.5	2.8/49.4 ($z = 0.1/0.5$)
RGB J0643+422	0.46	240	1282	0.181	0.200	0.369	32.7	9.5	-
RGB J0656+426	1.16	1960	9607	0.198	0.200	0.322	20.2	3.6	-
1ES 0735+178	−1.20	1259	6865	0.190	0.166	0.260	9.0	0.9	0.5
BZB J0809+3455	−0.24	252	1537	0.167	0.151	0.251	39.8	4.0	-
PKS 0829+046	−0.77	465	2465	0.196	0.240	0.379	10.1	2.7	0.6
Mrk 1218	2.44	1589	8994	0.165	0.166	0.280	43.1	5.7	-
OJ 287	0.97	2197	12966	0.166	0.182	0.296	17.4	2.6	3.1
B2 0912+29	3.49	3466	19492	0.167	0.138	0.228	45.9	3.6	1.6
1ES 0927+500	−0.18	2378	11404	0.209	0.182	0.346	11.0	2.8	-
RBS 0831	−0.31	394	2403	0.167	0.166	0.297	29.5	4.8	-
RGB J1012+424	0.18	270	1324	0.167	0.219	0.316	43.5	6.7	22.2
1ES 1028+511	1.16	4610	27154	0.167	0.182	0.305	12.4	2.0	1.4
RGB J1037+571	−1.53	790	3798	0.221	0.200	0.331	5.7	1.1	2.5 ($z = 0.6$)
RGB J1053+494	−0.76	1397	8567	0.167	0.200	0.386	6.4	2.2	0.5
RBS 0921	0.84	633	3534	0.173	0.240	0.354	20.1	4.2	-
RBS 0929	−0.62	923	4678	0.202	0.166	0.319	11.3	2.4	0.5/2.7 ($z = 0.1/0.5$)
1ES 1106+244	−1.65	200	1151	0.197	0.151	0.257	14.3	1.5	3.3
RX J1117.1+2014	0.16	2545	12950	0.190	0.151	0.281	12.5	1.8	0.18
1ES 1118+424	0.39	1685	9703	0.172	0.151	0.267	22.4	2.8	0.39
S4 1150+497	−0.53	749	4589	0.167	0.182	0.315	12.9	2.3	70.0
RGB J1231+287	0.74	1258	6664	0.185	0.138	0.243	36.6	3.5	12.2
1ES 1239+069	−0.86	224	1429	0.167	0.240	0.369	8.7	2.1	-
PG 1246+586	0.23	2123	12670	0.167	0.200	0.363	9.5	2.4	14.5 ($z = 0.73$)
1ES 1255+244	2.24	5127	29732	0.167	0.166	0.315	12.4	2.5	-
BZB J1309+4305	0.54	2359	14020	0.167	0.151	0.298	17.8	3.2	7.9
1FGL J1323.1+2942	0.24	1781	14622	0.121	0.151	0.243	18.0	1.6	1.2/3.7 ($z = 0.1/0.5$)
RX J1326.2+2933	1.36	1771	14150	0.127	0.166	0.256	17.8	1.7	-
RGB J1341+399	0.00	381	2286	0.167	0.200	0.405	12.7	5.1	-
RGB J1351+112	1.44	1715	8994	0.184	0.151	0.248	30.0	2.8	2.9 ($z = 0.62$)
RX J1353.4+5601	0.65	569	3163	0.175	0.200	0.339	24.8	5.3	-
RBS 1350	0.55	1387	8190	0.167	0.151	0.248	27.9	2.6	-
RBS 1366	1.89	1789	9843	0.173	0.200	0.327	17.1	3.3	7.9
1ES 1421+582	0.17	674	4016	0.167	0.219	0.378	13.2	3.8	-
RGB J1439+395	0.80	404	2321	0.167	0.151	0.246	62.4	5.7	5.0
1RXS J144053.2+061013	−0.09	424	2556	0.167	0.200	0.343	13.8	3.1	16.7
RBS 1452	0.03	1232	7474	0.165	0.151	0.254	25.9	2.7	0.5

Table 4
(Continued)

Source Name	σ	ON	OFF	α	E_{th} (TeV)	E_{dec} (TeV)	$UL_{@E_{dec}}$ (10^{-12} cm^{-2} s^{-1} TeV^{-1})	$UL_{>E_{th}}$ (% C.U.)	UL/Φ_{HE}
RGB J1532+302	−0.56	812	3648	0.227	0.166	0.348	10.7	3.0	-
RGB J1533+189	−1.44	653	4460	0.167	0.151	0.293	8.5	1.5	-
1ES 1533+535	0.54	191	973	0.188	0.182	0.324	41.7	8.9	-
RGB J1610+671B	−1.75	1318	6510	0.214	0.263	0.516	1.6	1.1	-
1ES 1627+402	−0.33	2191	13244	0.167	0.182	0.360	7.3	2.1	-
GB6 J1700+6830	−1.98	81	610	0.167	0.316	0.528	3.5	2.2	161
PKS 1717+177	0.42	934	4343	0.212	0.182	0.290	19.3	2.6	3.1($z = 0.58$)
PKS 1725+045	−0.58	41	271	0.167	0.200	0.329	37.5	7.3	127
PKS 1749+096	−1.00	64	438	0.167	0.166	0.257	43.6	4.3	1.6
RGB J1838+480	0.27	87	329	0.167	0.200	0.346	52.3	12.1	4.2
RGB J1903+556	0.19	164	968	0.167	0.240	0.398	22.4	7.0	22.2 ($z = 0.58$)
1FGL J1926.8+6153	0.62	231	1326	0.167	0.240	0.408	21.6	7.4	1.1/12.5 ($z = 0.1/0.5$)
PKS 2233-148	0.06	32	190	0.167	0.501	0.829	7.8	15.0	1.4e3 ($z = 0.49$)
3C 454.3	−1.21	220	981	0.25	0.138	0.250	23.0	2.5	0.6
RGB J2322+346	−0.42	518	2926	0.181	0.182	0.296	19.2	2.8	1.4
1ES 2321+419	2.05	992	3686	0.250	0.219	0.414	23.7	9.4	15.9 ($z = 0.5$)
B3 2322+396	−0.63	131	705	0.197	0.166	0.256	49.2	4.8	80 ($z = 1.05$)
1FGL J2329.2+3755	−0.13	847	5106	0.167	0.166	0.254	27.3	2.6	1.0/3.4 ($z = 0.1/0.5$)
1RXS J234332.5+343957	0.80	341	1952	0.167	0.151	0.250	53.5	5.2	3.2

Table 5
Results and Upper Limits for the Known VHE Sources

Source Name	σ	ON	OFF	α	E_{th} (TeV)	E_{dec} (TeV)	$UL_{@E_{dec}}$ (10^{-12} cm^{-2} s^{-1} TeV^{-1})	$UL_{>E_{th}}$ (% C.U.)	UL/Φ_{HE}
1ES 0033+595	3.23	4560	20321	0.214	0.288	0.490	10.0	5.4	0.8 ($z = 0.086$)
RGB J0152+017	1.83	1720	8693	0.188	0.240	0.376	14.1	3.6	1.2
RGB J0847+115	−0.03	3391	19889	0.171	0.182	0.338	8.63	2.0	0.3
RX J1136.5+6737	1.10	1324	7271	0.177	0.288	0.519	7.86	5.2	1.3
PKS 1222+216	3.40	7482	39770	0.180	0.182	0.257	24.1	2.2	0.2
3C 279	0.10	1479	8849	0.167	0.263	0.430	5.5	2.1	2.6
PKS 1510-089	2.00	2691	13698	0.167	0.263	0.496	4.7	2.9	1.1
RGB J1725+118	2.29	1979	10833	0.079	0.200	0.316	18.7	3.2	0.6/2.6 ($z = 0.1/0.5$)
0FGL J2001.0+4352	0.76	1102	6449	0.167	0.200	0.384	15.5	5.2	0.3 ($z = 0.2$)
RGB J2243+203	−0.12	1111	6458	0.173	0.166	0.263	19.3	2.1	0.3 ($z = 0.39$)
B3 2247+381	−0.93	1447	8042	0.185	0.166	0.315	8.8	1.8	0.5

5. PKS 1222+216 (FSRQ, $z = 0.432$).

   VHE emission from this FSRQ was detected by MAGIC in 2010 at a flux of the order of the Crab Nebula flux (Aleksić et al. 2011b). The detection of this VHE flare is of paramount importance for blazar physics: the rapid variability, and the fact that VHE photons can escape the bright photon field present in FSRQs was used to put constraints on the location of the γ-ray emitting region in blazars. The VERITAS non-detection constrains the low-flux state at a level of 2.2% Crab above 180 GeV. During 2014 May, PKS 1222+216 underwent another γ-ray flare, and VERITAS detected VHE emission at a flux of 3% Crab (Holder 2014a). A paper describing the VERITAS detection in 2014 is currently in preparation.
6. 3C 279 (FSRQ, $z = 0.536$).

   This quasar is the first of its class detected as a VHE emitter (Albert et al. 2008). VERITAS observations during 2011 were triggered by flaring activity observed at lower wavelengths (optical, X-rays, and HE γ-rays). The same flare triggered observations with the MAGIC telescopes (Aleksić et al. 2014c), which resulted as well in no VHE detection (flux upper limit equal to 1.7% Crab above 260 GeV). The VERITAS flux upper limit (2.1% Crab above 260 GeV) is similar to the one measured with the MAGIC telescopes.
7. PKS 1510-089 (FSRQ, $z = 0.361$).

   Two VHE flares from this quasar have been reported so far: the first during 2009 March–April, seen by H.E.S.S. (around 0.6% of the Crab Nebula flux above 260 GeV, see Abramowski et al. 2013a), the second during 2012 February, seen by MAGIC (around 1% of the Crab Nebula flux above 260 GeV, see Aleksić et al. 2014b). The VERITAS observations presented in this paper are quasi-simultaneous with both flares (see Table 2 for details). For the 2009 flare, VERITAS observations were taken a few days before the VHE flare seen by H.E.S.S. For the 2012 flare, VERITAS observations were taken every night from February 19 to 27, covering the *Fermi*-LAT flare. The VERITAS upper limit is 2.9% of the Crab Nebula flux above 260 GeV.
8. RGB J1725+118 (HBL, $z > 0.35$).

   The discovery of VHE emission from this blazar was recently reported by MAGIC (Cortina 2013) at a flux of 2% Crab above 140 GeV during observations in 2013 May triggered by an elevated optical state. No spectral

Table 6
Results and Upper Limits for the 2FGL Sources in the VERITAS Field of View

Source Name	σ	ON	OFF	α	$E_{\rm th}$ (TeV)	$E_{\rm dec}$ (TeV)	$\mathrm{UL}_{@E_{\rm dec}}$ (10^{-12} cm^{-2} s^{-1} TeV^{-1})	$\mathrm{UL}_{>E_{\rm th}}$ (% C.U.)	$\mathrm{UL}/\Phi_{\rm HE}$
2FGL J0047.9+2232	0.32	123	2058	0.0770	0.200	0.314	70.5	11.6	1.6e4
2FGL J0148.6+0127	1.15	1239	17272	0.063	0.240	0.412	25.1	8.9	6.7e3
2FGL J0158.4+0107	−1.62	582	13194	0.0625	0.240	0.435	16.6	7.1	150/2.2e3 ($z = 0.1/0.5$)
2FGL J0205.4+3211	1.76	232	3743	0.0524	0.166	0.290	102	15.4	5.4e5
2FGL J0212.1+5318	−1.22	389	8089	0.0512	0.200	0.377	37.8	11.9	1.0/9.1 ($z = 0.1/0.5$)
2FGL J0213.1+2245	0.57	501	7460	0.0655	0.182	0.295	63.3	9.2	29.3
2FGL J0326.1+2226	0.22	1342	25891	0.0515	0.151	0.249	92.9	9.0	2.5e4
2FGL J0440.4+1433	0.20	1028	19458	0.0525	0.182	0.340	50.3	12.1	60/416 ($z = 0.1/0.5$)
2FGL J0856.3+2058	0.19	1686	21961	0.0764	0.182	0.297	37.1	5.6	53 ($z = 0.5$)
2FGL J0929.5+5009	3.28	1712	17578	0.0884	0.200	0.349	40.2	9.6	28
2FGL J1058.4+0133	1.19	319	5882	0.0506	0.240	0.373	51.7	12.9	985
2FGL J1059.0+0222	−0.37	533	7097	0.0764	0.240	0.359	25.8	5.7	30/240 ($z = 0.1/0.5$)
2FGL J1141.0+6803	0.17	1195	12124	0.0981	0.288	0.525	7.5	5.1	0.7/18.9 ($z = 0.1/0.5$)
2FGL J1239.5+0728	1.41	198	2766	0.0644	0.240	0.368	55.1	13.1	67
2FGL J1245.1+5708	2.34	1418	24171	0.0545	0.219	0.369	40.7	10.8	276 ($z = 0.52$)
2FGL J1303.1+2435	0.33	3021	57951	0.0518	0.166	0.322	36.2	7.8	117
2FGL J1359.4+5541	1.74	507	5493	0.0850	0.219	0.347	50.5	10.8	1.4e5
2FGL J1722.7+1013	1.73	693	14010	0.0462	0.200	0.332	72.2	14.5	433
2FGL J1727.9+1220	−0.56	1816	23431	0.0789	0.200	0.315	15.3	2.5	41
2FGL J1927.5+6117	−1.94	127	1964	0.077	0.240	0.412	12.1	4.3	5.1/62 ($z = 0.1/0.5$)
2FGL J1959.9+4212	1.82	458	9118	0.037	0.219	0.347	64.4	13.8	24/176 ($z = 0.1/0.5$)

information is available at the present time. The VERITAS upper limit (3.2% Crab above 200 GeV) is consistent with the MAGIC measurement.

9. 0FGL J2001.0+4352 (HBL, $z = 0.18$:).
   Early results from *Fermi*-LAT indicated that this source was a good candidate for IACTs, in particular, due to its hard GeV spectrum (Abdo et al. 2009a). The MAGIC collaboration detected the source at a flux of ∼10% Crab during a single night (1.4 hr on 2010 July 16, see Aleksić et al. 2014a). The VERITAS upper limit clearly indicates that this blazar is variable at VHE, and that its baseline flux is below 5.2% Crab above 200 GeV.
10. RGB J2243+203 (HBL, $z > 0.39$).
    VHE emission from this source was detected by VERITAS during 2014 December, following a trigger from a high *Fermi*-LAT flux (Holder 2014b; Abeysekara 2015). Preliminary analysis indicates that the flux from the flaring blazar was at ∼4% Crab above 180 GeV. The upper limits computed from 2009 observations indicate that the VHE emission from this source is variable, being significantly lower (2.1% Crab above 170 GeV) than the 2014 detection.
11. B3 2247+381 (HBL, $z = 0.119$).
    This source was detected by MAGIC in 14 hours of observations from 2010 September to October, at a flux of 2.2% Crab above 170 GeV (Aleksić et al. 2012). The MAGIC observations were triggered by a high optical state, and there is evidence of variability in the simultaneous X-ray light curve. VERITAS observations do not cover the MAGIC detection, nor the high optical flux state measured by the *Tuorla* observatory. The non-detection by VERITAS (flux upper limit equal to 1.8% Crab above 170 GeV) constrains the low-state flux of this blazar to be lower than the MAGIC detection, suggesting that it may have been related to a VHE high-flux state.

In addition to these known VHE emitters, we discuss a few other targets with noteworthy histories.

1. 1ES 0037+405 (HBL, z unknown).
   VERITAS observations of this target were taken as a self-triggered ToO. During observations of the Andromeda galaxy (M31, see Bird 2015), a 4σ hotspot coincident with this blazar was observed in the reconstructed sky-map. However, further observations did not confirm the hotspot, and the cumulative significance is 1.5σ in 36 hr.
2. OJ 287 (LBL, $z = 0.306$).
   This blazar is one of the most studied objects of its kind due to a clear periodicity in its optical lightcurve, with a period of about 12 years. The VERITAS observations presented in this work cover the last active phase in Fall 2007 (from 2007 December 4 to 2008 January 1), with additional observations during 2010. The VHE upper limits are comparable to the ones measured with the MAGIC telescopes and presented by Seta et al. (2009).
3. 1FGL J1323.1+2942 (FSRQ, z unknown) and RX J1326.2+2933 (HBL, $z = 0.431$).
   Although the angular distance between the two sources is only 43′, they are not the same blazar. VERITAS can resolve the two objects, and they have been targeted by VERITAS independently (see last column of Table 1). Since they are well within the VERITAS FOV, the exposures on these two objects have been merged into a single data set.
4. B2 0912+29 (HBL, $z = 0.36$).
   This blazar shows the highest significance in our data set (3.5σ in 11.7 hr). This excess was confirmed at the same significance level by the cross-check analysis chain. Further observations were taken during the 2013 and 2014 observing seasons, but the initial excess did not increase. While VHE blazars are known to be variable,

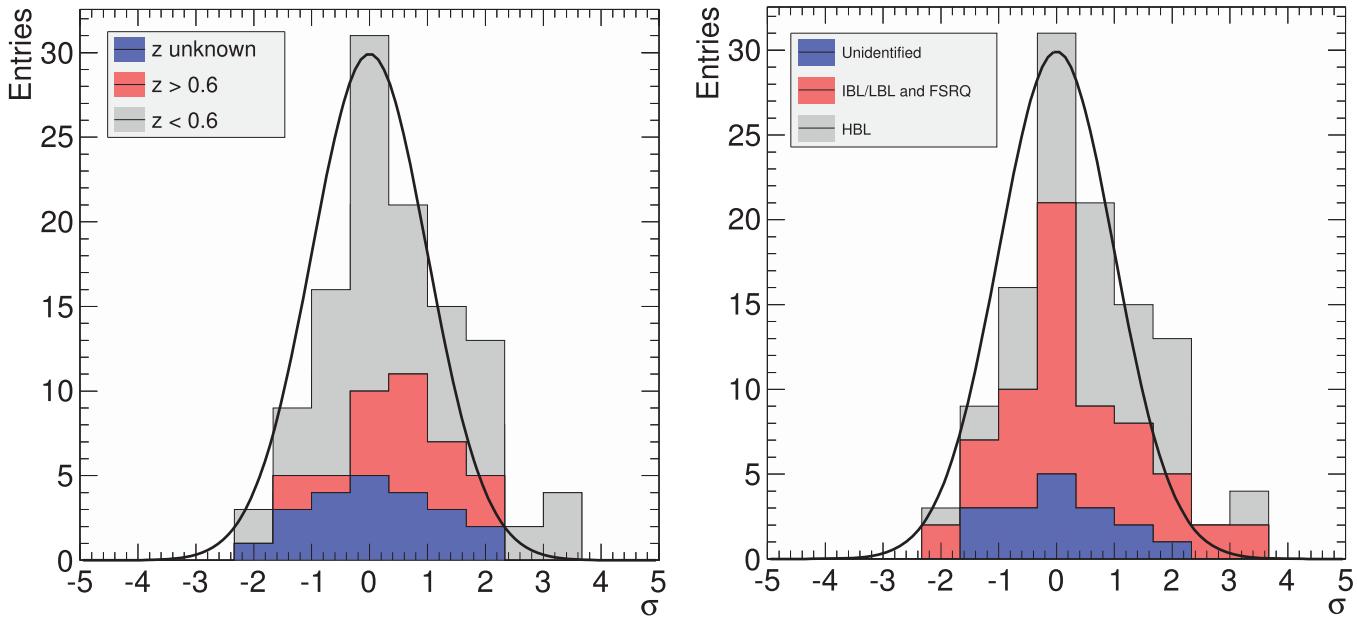

Figure 1. Left: stacked significance distribution of the sources included in our sample, classified according to their redshift. Sources with unknown z are in blue, sources with $z > 0.6$ are in red and sources with $z < 0.6$ are in gray. The Gaussian function represents the expectation from a randomly distributed sample, with mean equal to zero, and variance equal to 1. Right: same as the left panel, but for sources classified according to the AGN type. Unidentified sources are in blue, IBL/LBL/FSRQ in red, and HBL in gray.

and one could interpret the lack of a detection in 2013–2014 as due to variability, we also note that the probability of a 3.5σ excess reduces to only 2.0σ when 103 trials (the sources from Tables 1 and 3) are taken into account, and it is thus not enough to make any claim.

3.2. Significance Distributions

In Figure 1, we present the distribution of the significances for all the sources presented in our work. Given that the blazar population at VHE is not homogeneous (see the Introduction), and depends on both the blazar sub-class (which is correlated with the energy of the high-energy SED peak) and the blazar redshift (which implies a different level of EBL absorption), significance distributions are produced as a function of these two parameters. For the redshift division (left plot of Figure 1), redshifts lower or higher than 0.6 were considered, along with unknown redshift. Concerning the division of blazar sub-classes (right plot of Figure 1), the sources were categorized as HBLs, IBLs/LBLs/FSRQs, and blazars of unknown type. The Gaussian distribution expected from a sample with average $\hat{X} = 0$ and $\sigma = 1$ is overlaid on the significance distribution. A fit of the histogram with a Gaussian function instead yields $\hat{X} = 0.3 \pm 0.1$ and $\sigma = 1.2 \pm 0.1$.

4. STACKED ANALYSIS

Motivated by the skew in the significance distribution and in order to study if there is any evidence of emission from a population of blazars below the VERITAS sensitivity level, a stacked analysis of the data set is performed. For every source the γ-ray excess (ON—α OFF) and its uncertainty (the excess divided by the significance) are calculated. We then compute the sum of the excesses, and its uncertainty (the square root of the sum of the squared uncertainties), whose ratio provides the significance of the stacked excess. Sources known as VHE emitters are excluded from the stacked analysis, which only includes sources listed in Tables 1 and 3.

The stacked analysis indicates that there is evidence of VHE emission at a level of 4.0σ, corresponding to an excess of 1990 γ-rays. The same study is then performed for sub-samples of the overall data set. The majority of the excess (3.0σ) comes from nearby ($z < 0.6$) HBLs. On the other hand, the stacked analysis including only non-HBL sources located at an unknown distance or $z > 0.6$ results in a stacked significance of 1.1σ. However, because nearby HBLs are considered, the most likely VHE candidates, there are more of them and they often have deeper exposures. So this study has more sensitivity to the nearby HBLs. Indeed, the VERITAS exposure on HBLs located at $z < 0.6$ is about 196 hr. By assuming that the 4.0σ stacked excess comes from a constant signal from all sources in 570 hr, one would expect a 2.3σ excess in 196 hr. The excess from the $z < 0.6$ HBLs is thus compatible with this expectation, and it is not possible to claim that the stacked excess is dominated by a particular blazar population.

The MAGIC collaboration has also reported evidence for VHE emission from a stacked sample of IBL/HBL sources (Aleksić et al. 2011a), detecting a signal at a significance level of 4.9σ from an exposure of 394 hr. The following sources included in the present work are also part of the MAGIC sample: 1ES 0120+340, 1RXS J044127.8+150455, 1ES 0927 +500, 1ES 1028+511, RX J1117.1+2014, RX 1136.5+6737, and RBS 1366. The four sources with the highest significance in the MAGIC publication (1ES 0033+595, 1ES 1011+496, B2 1215+30, and 1ES 1741+196) were, notably, later confirmed as VHE emitters, either during flaring activity, or by increasing the integration time.

5. CONCLUSIONS

The results from the analysis of the observations of non-detected blazars targeted by VERITAS from 2007 to 2012 have been presented. In addition, γ-ray sources from the 2FGL

Table 7
Blazars Observed at the Lick Observatory using the Shane 3 m Kast Spectrograph

Target Name[a]	Obs. Date (UT)	Obs. Date (MJD—50000)	Exposure (s)	Signal to Noise[b]	Standard Star	z	Figure[c]
RBS 0082	2010 Aug 13	5421	3600	50, 77	BD+28 4211	⋯	2.2
1ES 0033+595	2012 Aug 22	6161	3600	20, 88	BD+28 4211	⋯	⋯
1ES 0033+595	2013 Dec 4	6630	3600	2.8, 34	G191B2B	⋯	2.2
1RXS J0045.3+2127	2012 Aug 22	6161	1800	56, 106	BD+28 4211	⋯	⋯
1RXS J0045.3+2127	2014 Oct 28	6958	1800	57, 121	Feige 110	⋯	2.2
RGB J0250+172	2010 Aug 15	5423	5400	21, 44	BD+28 4211	0.243	2.1
1ES 0446+449	2013 Feb 14	6337	3600	n/a, 65	HZ2	⋯	2.3
RGB J0505+612	2013 Feb 14	6337	900	0.4, 4.3	HZ2	⋯	2.3
2FGL J0540.4+5822	2014 Oct 28	6958	3600	14, 46	G19B2B	⋯	2.3
B2 0912+29	2013 Apr 7	6389	3600	57, 179	Feige 34	⋯	⋯
B2 0912+29	2013 Jan 4	6299	3600	81, 144	Feige 34	⋯	2.4
B2 0912+29	2013 Dec 4	6630	3600	48, 102	G191B2B	⋯	⋯
RBS 0929	2013 Apr 7	6389	3600	13, 33	Feige 34	⋯	2.4
RGB J1037+571	2013 Feb 14	6337	3600	54, 128	Feige 34		2.4
1ES 1118+424	2013 Feb 14	6337	3600	1.5, 22	Feige 34	0.230	2.1
PG 1246+586	2013 Apr 7	6389	3600	80, 229	GD 153	⋯	⋯
PG 1246+586	2014 May 29	6806	3600	86, 175	HZ44	⋯	⋯
PG 1246+586	2014 May 30	6807	3600	80, 203	HZ44	⋯	2.5
RBS 1366	2013 Apr 7	6389	900	7, 34	BD+33 2642	⋯	⋯
RBS 1366	2014 May 30	6807	3600	26, 72	BD+33 2642	0.237	2.1
1RXS J144053.2+061013	2013 Jan 4	6299	3800	13, 53	BD+33 2642	⋯	2.5
RGB J1725+118	2013 Jun 12	6455	3600	48, 129	BD+33 2642	⋯	⋯
RGB J1725+118	2014 May 29	6806	3600	81, 189	BD+33 2642	⋯	⋯
RGB J1725+118	2014 May 30	6807	3600	111, 205	BD+33 2642	⋯	2.5
RGB J1903+556	2013 Jun 13	6456	1800	18, 46	BD+28 4211		2.6
BZB J2243+2021	2010 Aug 13	5421	3600	92, 167	BD+28 4211	⋯	2.6
1ES 2321+419	2012 Aug 22	6161	3000	20, 33	BD+28 4211	⋯	⋯
1ES 2321+419	2014 Oct 28	6958	3600	52, 121	Feige 110	>0.267	2.1

Notes.
[a] See Table 1 in main text for coordinates.
[b] This is the average signal-to-noise per pixel. The first number is for the blue side CCD, between 3500 and 5400 A. The second number is for the red side CCD, between 5700 and 6800 Angstroms.
[c] Several targets have spectra from multiple nights. Only one spectrum per target is shown; this column indicates the corresponding figure, if applicable.

catalog that were within the FOV of these VERITAS observations were included in this study. For all the 114 sources included in this data set, we provided the VERITAS upper limit at VHE. Given that the redshift estimate of blazars is particularly important for VHE extragalactic astronomy, due to the γ-ray absorption on the EBL, we also presented the results from optical spectroscopy of 18 of these targets, determining the redshift for three of them, and providing a lower limit for the redshift of one of the sources.

We have presented the results from a stacked analysis of the data set, showing that there is some evidence of signal with a significance level of 4σ.

In the near future, the sensitivity of VHE astronomy will be significantly increased thanks to the Cherenkov Telescope Array (CTA), which will be capable of detecting sources with VHE fluxes of the order of 0.001 Crab units, about a factor of 10 better than current IACTs (Actis et al. 2011). Among the scientific goals of CTA, an important endeavor will be to increase the number of known VHE blazars in order to perform population studies. Among the VERITAS targets presented in this work, the sources with the highest significance could be considered as primary candidates for observations with CTA, which may be able to detect many of them on the basis of the extrapolation of their *Fermi*-LAT spectra to higher energies. The non-detection of a number of later detected VHE blazars emphasizes the variable nature of these sources, highlighting the importance of monitoring observations in order to increase the likelihood of catching the sources at detectable VHE states.

This research is supported by grants from the U.S. Department of Energy Office of Science, the U.S. National Science Foundation and the Smithsonian Institution, and by NSERC in Canada. We acknowledge the excellent work of the technical support staff at the Fred Lawrence Whipple Observatory and at the collaborating institutions in the construction and operation of the instrument. The VERITAS Collaboration is grateful to Trevor Weekes for his seminal contributions and leadership in the field of VHE gamma-ray astrophysics, which made this study possible. M.F. acknowledges support by the Science and Technology Facilities Council (grant number ST/L00075X/1).

APPENDIX
NEW REDSHIFT ESTIMATES

In this appendix, we present optical spectra of 18 blazars taken at the Lick Observatory in an attempt to spectroscopically measure their redshift. The sources selected for spectroscopy were selected independently from the sources selected in the

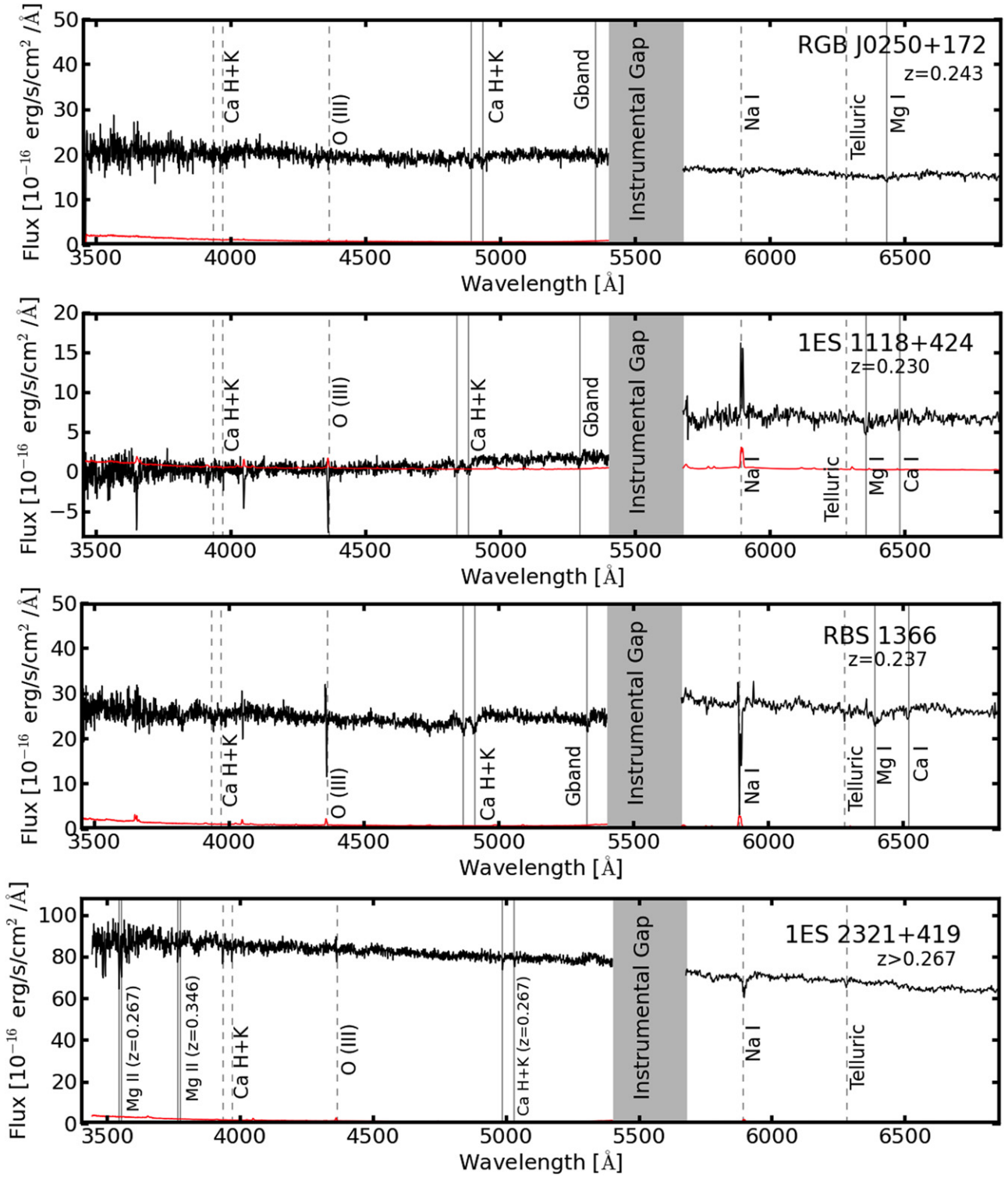

Figure 2. Spectra shown from top to bottom: RGB J0250+172 (2010 August 15), 1ES 1118+424 (2013 February 14), RBS 1366 (2014 May 30), 1ES 2321+419 (2014 October 28). Dashed lines indicate telluric and Galactic features. Red lines indicate the error array for each observation; some are not visible due to high S/N. Solid gray lines indicate features at non-zero redshift.

(The complete figure set (6 images) is available.)

main text, so the overlap is not complete. The spectra we show were taken between 2010 August and 2014 October. During the observations at Lick we often observed the same source more than once. Duplicate observations are noted in Table 7, but we only show one spectrum per source in the figures. Four of these spectra (shown in Figure 2) have host galaxy features that allow an accurate redshift determination, and are discussed in the main text.

REFERENCES

Abdo, A. A., Ackermann, M., Ajello, M., et al. 2009a, ApJS, 183, 46
Abdo, A. A., Ackermann, M., Ajello, M., et al. 2009b, ApJL, 707, L142
Abdo, A. A., Ackermann, M., Ajello, M., et al. 2010a, ApJS, 188, 405
Abdo, A. A., Ackermann, M., Agudo, I., et al. 2010b, ApJ, 716, 30
Abeysekara, A. U. 2015, Proc. ICRC, arXiv:1508.06334
Abeysekara, A. U., Archambault, S., Archer, A., et al. 2015, ApJL, 815, L22
Abramowski, A., Acero, F., Aharonian, F., et al. 2013a, A&A, 554, A107
Abramowski, A., Acero, F., Aharonian, F., et al. 2013b, A&A, 550, A4
Abramowski, A., Aharonian, F., Ait Benkhali, F., et al. 2014, A&A, 564, A9
Acciari, V. A., Aliu, E., Arlen, T., et al. 2010, ApJL, 708, L100
Ackermann, M., Ajello, M., Allafort, A., et al. 2012a, ApJ, 753, 83
Ackermann, M., Ajello, M., Ballet, J., et al. 2012b, ApJ, 751, 159
Actis, M., Agnetta, G., Aharonian, F., et al. 2011, ExA, 32, 193
Afanas'Ev, V. L., Dodonov, S. N., Moiseev, A. V., et al. 2005, ARep, 49, 374
Aharonian, F., Akhperjanian, A., Beilicke, M., et al. 2004, A&A, 421, 529
Aharonian, F., Akhperjanian, A. G., Bazer-Bachi, A. R., et al. 2005, A&A, 441, 465
Aharonian, F., Akhperjanian, A. G., Barres de Almeida, U., et al. 2008a, A&A, 481, L103
Aharonian, F., Akhperjanian, A. G., Barres de Almeida, U., et al. 2008b, A&A, 478, 387
Ahnen, M. L., Ansoldi, S., Antonelli, L. A., et al. 2015, ApJL, 815, L23
Ajello, M., Romani, R. W., Gasparrini, D., et al. 2014, ApJ, 780, 73
Albert, J., Aliu, E., Anderhub, H., et al. 2008, Sci, 320, 1752
Aleksić, J., Antonelli, L. A., Antoranz, P., et al. 2011a, ApJ, 729, 115
Aleksić, J., Antonelli, L. A., Antoranz, P., et al. 2011b, ApJL, 730, L8
Aleksić, J., Alvarez, E. A., Antonelli, L. A., et al. 2012, A&A, 539, A118
Aleksić, J., Ansoldi, S., Antonelli, L. A., et al. 2014a, A&A, 572, A121
Aleksić, J., Ansoldi, S., Antonelli, L. A., et al. 2014b, A&A, 569, A46
Aleksić, J., Ansoldi, S., Antonelli, L. A., et al. 2014c, A&A, 567, A41
Aleksić, J., Ansoldi, S., Antonelli, L. A., et al. 2015a, MNRAS, 446, 217
Aleksić, J., Ansoldi, S., Antonelli, L. A., et al. 2015b, JHEAp, 5, 30
Aliu, E., Archambault, S., Arlen, T., et al. 2012, ApJ, 759, 102
Angel, J. R. P., & Stockman, H. S. 1980, ARA&A, 18, 321
Archambault, S., Arlen, T., Aune, T., et al. 2013, ApJ, 776, 69
Archambault, S., Aune, T., Behera, B., et al. 2014, ApJL, 785, L16
Archambault, S., Archer, A., Beilicke, M., et al. 2015, ApJ, 808, 110
Atwood, W. B., Abdo, A. A., Ackermann, M., et al. 2009, ApJ, 697, 1071
Bade, N., Fink, H. H., & Engels, D. 1994, A&A, 286, 381
Bauer, F. E., Condon, J. J., Thuan, T. X., & Broderick, J. J. 2000, ApJS, 129, 547
Benbow, W. 2015, Proc. ICRC, arXiv:1508.07251
Bird, R. 2015, Proc. ICRC, arXiv:1508.07195
Böhringer, H., Voges, W., Huchra, J. P., et al. 2000, ApJS, 129, 435
Brinkmann, W., Siebert, J., Feigelson, E. D., et al. 1997, A&A, 323, 739
Burbidge, E. M., & Kinman, T. D. 1966, ApJ, 145, 654
Burbidge, G. R., Crowne, A. H., & Smith, H. E. 1977, ApJS, 33, 113
Cao, L., Wei, J.-Y., & Hu, J.-Y. 1999, A&AS, 135, 243
Carswell, R. F., Strittmatter, P. A., Williams, R. E., Kinman, T. D., & Serkowski, K. 1974, ApJL, 190, L101
Chandra, S., Baliyan, K. S., Ganesh, S., & Joshi, U. C. 2012, ApJ, 746, 92
Cohen, R. D., Smith, H. E., Junkkarinen, V. T., & Burbidge, E. M. 1987, ApJ, 318, 577
Cornwell, T. J., Saikia, D. J., Shastri, P., et al. 1986, JApA, 7, 119
Cortina, J. 2013, ATel, 5080, 1
Costamante, L. 2007, Ap&SS, 309, 487
Costamante, L., & Ghisellini, G. 2002, A&A, 384, 56
Doert, M., & Errando, M. 2014, ApJ, 782, 41
Drinkwater, M. J., Webster, R. L., Francis, P. J., et al. 1997, MNRAS, 284, 85
Eracleous, M., & Halpern, J. P. 2004, ApJS, 150, 181
Errando, M. 2011, Proc. ICRC, 8, 133
Falcone, A. D., Bond, I. H., Boyle, P. J., et al. 2004, ApJ, 613, 710
Falomo, R. 1991, AJ, 102, 1991
Falomo, R., & Kotilainen, J. K. 1999, A&A, 352, 85
Fanaroff, B. L., & Riley, J. M. 1974, MNRAS, 167, 31
Fischer, J.-U., Hasinger, G., Schwope, A. D., et al. 1998, AN, 319, 347
Fomin, V. P., Stepanian, A. A., Lamb, R. C., et al. 1994, APh, 2, 137
Franceschini, A., Rodighiero, G., & Vaccari, M. 2008, A&A, 487, 837
Fumagalli, M., Dessauges-Zavadsky, M., Furniss, A., et al. 2012, MNRAS, 424, 2276
Furniss, A., Williams, D. A., Danforth, C., et al. 2013, ApJL, 768, L31
Ghisellini, G., Tagliaferri, G., Foschini, L., et al. 2011, MNRAS, 411, 901
Giommi, P., Piranomonte, S., Perri, M., & Padovani, P. 2005, A&A, 434, 385
Giommi, P., Polenta, G., Lähteenmäki, A., et al. 2012, A&A, 541, A160
Glikman, E., Helfand, D. J., White, R. L., et al. 2007, ApJ, 667, 673
Halpern, J. P., Impey, C. D., Bothun, G. D., et al. 1986, ApJ, 302, 711
Healey, S. E., Romani, R. W., Cotter, G., et al. 2008, ApJS, 175, 97
Henstock, D. R., Browne, I. W. A., Wilkinson, P. N., & McMahon, R. G. 1997, MNRAS, 290, 380
Hewitt, A., & Burbidge, G. 1993, ApJS, 87, 451
Hillas, A. M. 1985, Proc. ICRC, 3, 445
Hillas, A. M., Akerlof, C. W., Biller, S. D., et al. 1998, ApJ, 503, 744
Holder, J. 2011, Proc. ICRC, 12, 137
Holder, J. 2014a, ATel, 5981, 1
Holder, J. 2014b, ATel, 6849, 1
Holder, J., Atkins, R. W., Badran, H. M., et al. 2006, APh, 25, 391
Horan, D., Badran, H. M., Bond, I. H., et al. 2004, ApJ, 603, 51
Impey, C. D., & Neugebauer, G. 1988, AJ, 95, 307
Jannuzi, B. T., Smith, P. S., & Elston, R. 1993, ApJS, 85, 265
Kieda, D. B. 2013, Proc. ICRC, arXiv:1308.4849
Komossa, S., Voges, W., Xu, D., et al. 2006, AJ, 132, 531
Konigl, A. 1981, ApJ, 243, 700
Kraus, J. D., & Gearhart, M. R. 1975, AJ, 80, 1
Landoni, M., Falomo, R., Treves, A., & Sbarufatti, B. 2014, A&A, 570, A126
Laurent-Muehleisen, S. A., Kollgaard, R. I., Ciardullo, R., et al. 1998, ApJS, 118, 127
Laurent-Muehleisen, S. A., Kollgaard, R. I., Feigelson, E. D., Brinkmann, W., & Siebert, J. 1999, ApJ, 525, 127
Lavaux, G., & Hudson, M. J. 2011, MNRAS, 416, 2840
Lawrence, C. R., Pearson, T. J., Readhead, A. C. S., & Unwin, S. C. 1986, AJ, 91, 494
Li, H. Z., Xie, G. Z., Yi, T. F., Chen, L. E., & Dai, H. 2010, ApJ, 709, 1407
Li, T.-P., & Ma, Y.-Q. 1983, ApJ, 272, 317
Lister, M. L., Aller, M., Aller, H., et al. 2011, ApJ, 742, 27
Marcha, M. J. M., Browne, I. W. A., Impey, C. D., & Smith, P. S. 1996, MNRAS, 281, 425
Marziani, P., Sulentic, J. W., Dultzin-Hacyan, D., Calvani, M., & Moles, M. 1996, ApJS, 104, 37
Maselli, A., Massaro, E., Nesci, R., et al. 2010, A&A, 512, A74
Massaro, E., Giommi, P., Leto, C., et al. 2009, A&A, 495, 691
Massaro, E., Giommi, P., Perri, M., et al. 2003, A&A, 399, 33
Massaro, F., D'Abrusco, R., Tosti, G., et al. 2012, ApJ, 750, 138
Meisner, A. M., & Romani, R. W. 2010, ApJ, 712, 14
Mirabal, N., Frías-Martinez, V., Hassan, T., & Frías-Martinez, E. 2012, MNRAS, 424, L64
Mirzoyan, R. 2014a, ATel, 6062, 1
Mirzoyan, R. 2014b, ATel, 6349, 1
Mirzoyan, R. 2014c, ATel, 5768, 1
Mücke, A., & Protheroe, R. J. 2001, APh, 15, 121
Mukherjee, R. 2001, in AIP Conf. Ser. 558, High Energy Gamma-ray Astronomy, ed. F. A. Aharonian, & H. J. Völk (Melville, NY: AIP), 324
Muriel, H., Donzelli, C., Rovero, A. C., & Pichel, A. 2015, A&A, 574, A101
Nieppola, E., Tornikoski, M., & Valtaoja, E. 2006, A&A, 445, 441
Nilsson, K., Pursimo, T., Heidt, J., et al. 2003, A&A, 400, 95
Nolan, P. L., Abdo, A. A., Ackermann, M., et al. 2012, ApJS, 199, 31
Osterbrock, D. E., & Dahari, O. 1983, ApJ, 273, 478
Padovani, P. 1992, A&A, 256, 399
Padovani, P., Costamante, L., Ghisellini, G., Giommi, P., & Perlman, E. 2002, ApJ, 581, 895
Padovani, P., & Giommi, P. 1995a, MNRAS, 277, 1477
Padovani, P., & Giommi, P. 1995b, ApJ, 444, 567
Perlman, E. S. 2000, in AIP Conf. Ser. 515, GeV-TeV Gamma Ray Astrophysics Workshop:Towards a Major Atmospheric Cherenkov Detector VI, ed. B. L. Dingus, M. H. Salamon, & D. B. Kieda (Melville, NY: AIP), 53
Perlman, E. S., Stocke, J. T., Schachter, J. F., et al. 1996, ApJS, 104, 251
Piranomonte, S., Perri, M., Giommi, P., Landt, H., & Padovani, P. 2007, A&A, 470, 787
Piron, F. 2000, PhD thesis, Univ. Paris-Sud
Plotkin, R. M., Anderson, S. F., Brandt, W. N., et al. 2010, AJ, 139, 390
Rani, B., Gupta, A. C., Bachev, R., et al. 2011, MNRAS, 417, 1881
Rau, A., Schady, P., Greiner, J., et al. 2012, A&A, 538, A26
Rolke, W. A., López, A. M., & Conrad, J. 2005, NIMPA, 551, 493
Salamon, M. H., & Stecker, F. W. 1998, ApJ, 493, 547
Sandrinelli, A., Treves, A., Falomo, R., et al. 2013, AJ, 146, 163
Sbarufatti, B., Treves, A., Decarli, R., et al. 2009, ATel, 2123, 1
Sbarufatti, B., Treves, A., Falomo, R., et al. 2005, AJ, 129, 559
Sbarufatti, B., Treves, A., Falomo, R., et al. 2006, AJ, 132, 1
Seta, H., Isobe, N., Tashiro, M. S., et al. 2009, PASJ, 61, 1011

Şentürk, G. D., Errando, M., Böttcher, M., & Mukherjee, R. 2013, ApJ, 764, 119
Shaw, M. S., Romani, R. W., Cotter, G., et al. 2012, ApJ, 748, 49
Shaw, M. S., Romani, R. W., Cotter, G., et al. 2013, ApJ, 764, 135
Shaw, M. S., Romani, R. W., Healey, S. E., et al. 2009, ApJ, 704, 477
Sikora, M., Begelman, M. C., & Rees, M. J. 1994, ApJ, 421, 153
Smith, H. E., Smith, E. O., & Spinrad, H. 1976, PASP, 88, 621
Sol, H., Zech, A., Boisson, C., et al. 2013, APh, 43, 215
Sowards-Emmerd, D., Romani, R. W., Michelson, P. F., Healey, S. E., & Nolan, P. L. 2005, ApJ, 626, 95
Stecker, F. W., de Jager, O. C., & Salamon, M. H. 1996, ApJL, 473, L75
Stickel, M., Fried, J. W., & Kuehr, H. 1988, A&A, 191, L16
Stickel, M., Fried, J. W., & Kuehr, H. 1989, A&AS, 80, 103
Stickel, M., Padovani, P., Urry, C. M., Fried, J. W., & Kuehr, H. 1991, ApJ, 374, 431
Stocke, J. T., Morris, S. L., Gioia, I. M., et al. 1991, ApJS, 76, 813
Taylor, A. M., Vovk, I., & Neronov, A. 2011, A&A, 529, A144
Thompson, D. J., Djorgovski, S., & de Carvalho, R. 1990, PASP, 102, 1235
Turriziani, S., Cavazzuti, E., & Giommi, P. 2007, A&A, 472, 699
Urry, C. M., & Padovani, P. 1995, PASP, 107, 803
White, G. L., Jauncey, D. L., Wright, A. E., et al. 1988, ApJ, 327, 561
White, R. L., Becker, R. H., Gregg, M. D., et al. 2000, ApJS, 126, 133
Williams, D. A. 2005, in AIP Conf. Ser. 745, High Energy Gamma-Ray Astronomy, ed. F. A. Aharonian, H. J. Völk, & D. Horns (Melville, NY: AIP), 499